NOTICE: When government or other drawings, specifications or other data are used for any purpose other than in connection with a definitely related government procurement operation, the U. S. Government thereby incurs no responsibility, nor any obligation whatsoever; and the fact that the Government may have formulated, furnished, or in any way supplied the said drawings, specifications, or other data is not to be regarded by implication or otherwise as in any manner licensing the holder or any other person or corporation, or conveying any rights or permission to manufacture, use or sell any patented invention that may in any way be related thereto.

AFCRC-TN-60-173

10

A REVIEW OF THEORIES AND MEASUREMENTS OF RADAR GROUND RETURN

by

Edward A. Wolff

Scientific Report No. 1
on
Contract AF19(604)-5198

Prepared for
ELECTRONICS RESEARCH DIRECTORATE
AIR FORCE CAMBRIDGE RESEARCH CENTER
AIR RESEARCH AND DEVELOPMENT COMMAND
BEDFORD, MASSACHUSETTS

Report No. CRC-5198-2
Feb. 29, 1960

ELECTROMAGNETIC RESEARCH CORPORATION
SHERATON BUILDING, 711-14th ST., N. W.
WASHINGTON 5, D. C.

AFCRC- TN-60-173

A REVIEW OF THEORIES AND MEASUREMENTS OF RADAR GROUND RETURN

by

Edward A. Wolff

Scientific Report No. 1
on
Contract AF19(604)-5198

Prepared for
ELECTRONICS RESEARCH DIRECTORATE
AIR FORCE CAMBRIDGE RESEARCH CENTER
AIR RESEARCH AND DEVELOPMENT COMMAND
BEDFORD, MASSACHUSETTS

ELECTROMAGNETIC RESEARCH CORPORATION
SHERATON BUILDING, 711-14th ST., N.W.
WASHINGTON 5, D. C.

Report No. CRC-5198-2
Feb. 29, 1960

Requests for additional copies by Agencies of the Department of Defense, their contractors, and other Government agencies should be directed to the

Armed Services Technical Information Agency
Arlington Hall Station
Arlington 12, Virginia

Department of Defense contractors must be established for ASTIA services or have their "need-to-know" certified by the cognizant military agency of their project or contract.

All other persons and organizations should apply to the

U. S. Department of Commerce
Office of Technical Services
Washington 25, D. C.

ABSTRACT

A summary of the principal sea and ground clutter measurement programs is presented and their results are compared. The principal theoretical work is reviewed for both sea and ground return. The theories reviewed include the corrugated surface, drop, and facet theories of sea clutter and the slightly rough surface and thin lossy cylinder theories of ground clutter. In addition, several miscellaneous theories based upon hypothetical statistical descriptions of the surface (such as arrays of spheres) are discussed. A comparison of the theoretical conclusions with the experimental results is made for each theory and the present status of our understanding of ground return is reviewed.

TABLE OF CONTENTS

LIST OF ILLUSTRATIONS

Figure

24. Ground return, pasture, K_a Band

25. Geometry for facets

26. Geometry for facets aligned with the wind

27. Curve of $\Sigma(b_n B)^{2n}$

1.0 INTRODUCTION.

1.1 The Clutter Problem.

The propagation of electromagnetic waves over a rough surface has been a subject of interest for many years. This interest was greatly intensified by the advent of radar practice. In radar, the scattering of waves from the ground can be either detrimental or beneficial. For example, in detection or tracking of targets on or near the surface, it is necessary to be able to distinguish the target from the background clutter due to reflections from the surface itself. In such applications, the ground return is detrimental to the desired operation of the radar system. On the other hand, in navigation, position location, and reconnaissance by ground mapping, the ground return itself is the desired "target" information, and the most important characteristic is the contrast obtainable between objects (such as buildings, for example,) and their immediate surroundings. Consequently, in order to design radar systems intelligently, a knowledge of ground return characteristics is required.

For distributed targets like terrain or the sea, the size of the target depends on the radar parameters; in particular, the target area illuminated depends on the antenna beamwidth and the pulse length. In exploring scattering mechanisms, it is desirable to be able to normalize the measured power to a value which is independent of the radar parameters. This can be done when the scattering properties are uniform over the illuminated area, in which case the scattering is said to be area-extensive. By dividing the radar area by the illuminated area, Goldstein [1, p.] * introduced the dimensionless quantity

---

* Numbers in square brackets refer to the References in Section 7.0

$$\sigma^\circ = \frac{\sigma}{A}, \qquad (1.1)$$

where A is the area illuminated by the radar beam, and σ is the radar area, which is defined by the familiar radar equation

$$P_r = \frac{P_t G^2 \lambda^2}{(4\pi)^3 R^4} F^4 \sigma, \qquad (1.2)$$

in which P_r and P_t are the received and transmitted powers, respectively, G is the radar antenna gain, R is the distance between the radar and the target, and F is the illumination factor describing the interference pattern due to the direct and ground reflected waves. In most work, F is assumed to be unity.

One research group (Ohio State University Antenna Laboratory) uses a modified quantity related to σ°, which is obtained by dividing σ by the projection of the illuminated area normal to the radar beam direction. This quantity, for which they use the symbol γ, thus is equal to

$$\gamma = \frac{\sigma^\circ}{\sin\Theta}, \qquad (1.3)$$

where Θ is the elevation angle of the incident beam.

Although σ° strictly should be used only for homogeneous scattering surfaces, nevertheless the tendency has been to use it even for heterogeneous scatterers. In such cases, the value of σ° deduced is some average of the varying scattering function over the illuminated area. Thus when we speak in terms of the quantity σ°, what usually will be meant is this average value.

In general, σ° is a function of the characteristics of the incident wave and the nature of the surface. The wave characteristics which are of importance are the frequency, polarization, and the depression angle (or elevation angle at the ground). The surface properties which are of importance are many in number and variety. These are roughly divisible into two categories, the <u>form</u> of the surface, and its electrical properties. Under the

surface form are included such characteristics as ground contour, and protuberances such as vegetation, trees, buildings, vehicles, and animals. The electrical properties are the dielectric constant and conductivity (and sometimes the permeability), which, in turn, depend significantly on moisture content for many types of terrain elements. It is evident, therefore, that the clutter problem involves a large number of variables. If other than a purely empirical approach to the problem is to be made, it is necessary to determine the nature of the controlling mechanisms. If this can be done, then it should be possible to predict characteristics of the environment in which a radar is being designed to operate.

1.2 Organisation of the Report.

The purpose of this report is to give a summary of the principal investigations which have been made of the clutter problem. This will include experimental measurement programs, as well as theories which have been advanced to explain the observations. In particular, we shall attempt to point out the underlying assumptions (explicit or implicit) wherever possible. Comparison of the theoretical and experimental results will be made in order to arrive at a measure of usefulness.

Some of the papers covered by this review are classified. To avoid classification of the entire report, it was decided to segregate the discussion of the classified papers into a classified supplement. In this way, the bulk of the material could be communicated in an unclassified report. Although this is not the most desirable course from the standpoint of a unified presentation, nevertheless it was felt that the greater freedom in distribution and use of an unclassified review of the field would outweigh the disadvantage of a separate

coverage of the classified work.

The experimental results will be presented first, in order to bring out the essential features which a successful theory must reveal. This will be presented in Sec. 2. Of necessity, this portion of the present report will be incomplete, since it does not include the results which are classified. In Sec. 3 through Sec. 5, various theoretical treatments will be discussed, and their results compared with the available experimental evidence. This will be followed by a general summary of the "state of the art" with respect to the present understanding of the phenomenon of ground return.

2.0 REVIEW OF EXPERIMENTAL RESULTS.

2.1 General.

The return from the sea and from many different types of land has been measured by several organizations in an endeavor to obtain information on the nature of the return and the effect of the various parameters on which it depends. The radar cross section per unit area of ground is a function of the frequency, polarization and angle of incidence of the electromagnetic wave. The cross section also depends upon the surface roughness and the wind. Sea return depends upon the angle between the direction of propagation and the wind direction. Ground return depends upon the composition and size of the objects above the ground and their water content. The results of the measurements which have been made to determine the effects of these parameters are described below.

2.2 Measurement Programs.

Measurements of radar back scattering have been undertaken by many organizations both in this country and abroad. Some of the more important

measurement programs are described and their results are compared. In some instances these results are inconsistent. Unfortunately, insufficient information is generally given regarding system accuracies and methods of calibration, so that it is not possible to determine whether the inconsistency is due to the equipment or to differences in the actual parameters measured. Also, there is no overabundance of measured data. The experimental programs are described below in approximately chronological order. The important results of these measurements are then compared to determine the manner in which σ° is affected by the various parameters.

2.2.1 MIT Radiation Laboratory.

The results of measurements made by the Radiation Laboratory appear in the literature in several places [2, 3, 4].

These measurements were made along the New England coast at elevations from 70 to 120 feet and at wavelengths from 9.2 to 1.25 cm. The measurements include depression angles from 0.3° to 2°, and include sea states from slight chop to rough seas with 14 foot waves. The results of these measurements show that for calm seas the return for vertical polarization can be as much as 30 db greater than the return for horizontal polarization at 9.2 and 3.2 cm. The accuracy of the measurements is given as 2 db at 3.2 and 9.2 cm. This suggests that interference lobes caused by reflections from the surface play a role in the back-scattering process.

The measurements also show that the σ° versus depression angle (Θ) curves have a large slope for small values of Θ and a smaller slope at intermediate values of Θ. The angle at which this slope changes is called the critical angle and varies from 1 degree for rough seas to 5 degrees for calm

sea: [4, p.510].

2.2.2 Dominion Physical Laboratory.

The Doppler shift of energy reflected from the sea has been measured at 13.56 megacycles in New Zealand [5]. The equipment used to make these measurements is not described. A typical spectrum made with a wave analyzer is shown in Fig. 1. This spectrum is explained by assuming the reflection is from a diffraction grating moving with the velocity of waves whose length is $\lambda/2$ where λ is the radar wavelength.

2.2.3 Naval Research Laboratory, Wave Propagation Branch.

The Wave Propagation Branch used airborne radars for the measurement of sea clutter for several years. These radars operated at 1250 mc, 3300 mc, and 9300 mc, and were mounted beneath the wings of the aircraft. The aircraft also contained meteorological instruments, and oceanographic measurements were made of the sea simultaneously with the radar measurements. The radars were capable of measuring the sea clutter simultaneously at all the frequencies and were capable of measuring the reflected power on the transmitted polarization and the orthogonal polarisation [6,7,8]. The results of measurements made in October 1955 are shown in Figs. 2 and 3. The results of similar measurements made in January 1956 are shown in Figs. 4--7. These measurements indicate that σ^o is greater for vertical polarization, higher wind speed, and normal incidence. Later measurements show that σ^o is proportional to Θ^4 in the interval from 1 to 14 degrees as shown in Fig. 8 [9]. These measurements can be explained qualitatively at low depression angles by the presence of interference lobes and at high angles by the existence of reflecting areas aligned perpendicular to the incident wave normal.

2.2.4 Johns Hopkins University Radiation Laboratory.

Johns Hopkins University Radiation Laboratory made sea clutter measurements from the bow of a ship in the Atlantic Ocean in November 1955. Measurements ~~were~~ made at 9.6, 24, 35, and 49 kmc. The measurements on each frequency were made simultaneously. Measurements were made on vertical, horizontal and circular polarization. The sea varied from calm with 4 to 10 knot winds to moderately heavy with a 26 knot wind [10]. Some of the measured results are shown in Figs. 9 and 10. Fig. 9 shows that the variation of σ° with depression angle has the same characteristics from 9.6 to 35 kmc. Fig. 10 shows that the variation of σ° with frequency is constant for depression angles above 70°.

2.2.5 MIT Lincoln Laboratory.

The MIT Lincoln Laboratory made sea clutter measurements at 18 and 24 megacycles in January 1955 [11,12]. The measurements were made from a shore installation at Plum Island. These measurements indicate a value of of approximately -43 db, an average doppler frequency of about 0.42 cycle per second at 18.39 mc and a doppler frequency of 0.5 cycle per second at 24.7 mc. This indicates the reflection at these frequencies is from a diffraction grating moving with the velocity of waves whose length is half the radar wavelength.

2.2.6 Naval Research Laboratory, Radio Astronomy Branch.

NRL made back scattering measurements over water from a bridge across the Potomac River, and made measurements over land from approaches to bridges in Louisiana and Texas. Measurements were made at wavelengths of 3.2 cm, 1.25 cm and 8.6 mm. However, these measurements were not made simultaneously. The measurements covered depression angles from 10° to 90° [13].

The results of these measurements are shown in Figs. 11 -- 18. These Figures indicate that σ° for sea clutter varies as λ^{-1} below a depression angle of 60° and near normal incidence. The ground clutter measurements indicate a strong dependence upon the type of vegetation and the moisture content of that vegetation.

2.2.7 Georgia Institute of Technology Engineering Experiment Station.

The Georgia Institute of Technology made sea return measurements during 1955 from a tower at Boca Raton, Florida [14]. Measurements were made at 6.3 and 35 kmc with antenna heights between 35 and 124 feet above the sea surface. The sea is described as generally consisting of short-crested waves covered with chop, with occasional swell. This study indicates that for depression angles below 4° empirical formulas can be fitted to the measured data at 6.3 and 35 kmc which indicate that σ° varies as $W^{3.2}$ for horizontal polarization and as $W^{2.0}$ for vertical polarization where W is the wind speed in knots. These experiments also show that the spectrum at 35 kmc is five times as wide as the spectrum 6.3 kmc.

2.2.8 University of Illinois Control Systems Laboratory.

The Control Systems Laboratory measured sea clutter near the New England coast with an airborne coherent X-band radar in the fall of 1954. The aircraft altitude was varied from 500 to 2500 feet. The measurements were made at depression angles between 0.4° and 20°. The aircraft flew at an air speed of about 150 knots with the radar antenna fixed in the direction of the ground track, by adjusting it for maximum doppler frequency shift. The radar return from a 250-foot range interval was gated for recording [15]. These measurements indicate that for calm seas the doppler spectrum is symmetrical

in shape. For rough seas the spectrum is unsymmetrical, with the downwind-moving scatterers contributing to the broader side of the spectrum. This can be explained by assuming the back scattering takes place from facets whose slope distribution is unsymmetrical along the upwind-downwind axis.

2.2.9 Ohio State University Antenna Laboratory.

Measurements of radar back scattering from land have been made by the Antenna Laboratory at 10, 15.5 and 35 kmc with horizontal and vertical polarization from a boom mounted on a truck. Measurements were made simultaneously at the three frequencies for various types of terrain, such as concrete and asphalt roads, tall and short dry and wet grass, and plowed fields [16]. These measurements show that for smooth ground σ° decreases rapidly with depression angle and may decrease as much as 25 db from 80° to 20°, while for rough ground the decrease may be less than 5 db. This indicates the possible influence of interference lobes. For smooth ground, such as concrete and asphalt roads, σ° varies approximately as λ^{-2}, while it varies as λ^{-1} for two-inch grass. Also, for smooth ground σ° is 5 to 10 db greater for vertical polarization than for horizontal polarization for a depression angle of 20°, and less than 5 db greater at a depression angle of 80° at 35 kmc. For rough ground there is little dependence of σ° on polarization.

2.2.10 Johns Hopkins University Applied Physics Laboratory.

The Applied Physics Laboratory made measurements of the return from grassland from 9.4 kmc to 35 kmc using both horizontal and vertical polarization [17]. These measurements were made from a 35-foot tower and included depression angles from 15° to 65°. The terrain is described as nearly level

pasture with mixed green grass from 12 to 16 inches high before mowing, and 4 inches high after mowing. These measurements indicate that σ° is 2.5 db greater on vertical than horizontal polarization at 9.4 kmc, 1.5 db greater at 16.5 kmc and 1.5 db less at 35 kmc.

2.3 Comparison of Experimental Results for Sea Return.

The measurements which have been performed have yielded data on the effect of the various parameters on the return from water. In order to obtain a picture of the effects of these factors, the data from the measurements is compared for each of the parameters. The variation of σ° with frequency, polarization, depression angle, and wind speed and direction is examined. Also, the measurements of the characteristics of clutter fluctuations will be discussed.

2.3.1 Variation of σ° with Frequency.

The manner in which σ° varies with frequency depends upon the other parameters which affect σ°. Recent measurements of sea clutter taken from the bow of a ship are shown in Fig. 9. These measurements indicate that σ° is independent of frequency for depression angles greater than 70° for vertical polarization. Similar results were found for horizontal polarization. For smaller depression angles the variation depends upon the sea state; σ° varies from about λ^{-4} for calm seas to λ^{0} for rough seas for frequencies between 10 and 50 kmc [10, p.235; 3, p.944; 4, p.511]. The results of water measurements made from a bridge are shown in Fig. 11 [13, p.977]. From Fig. 11 it can be seen that below a depression angle of 60° the variation of σ° with wavelength is proportional to λ^{-1} from 10 to 35 kmc. Fig. 11

also indicates that σ° varies as λ^{-1} near vertical incidence, but that the frequency dependence is less obvious at intermediate angles near 60°.

2.3.2 Variation of σ° with Polarization.

The return from the sea depends upon the sea state. For calm seas the return for vertical polarization can be as much as 20 to 30 db greater than the return for horizontal polarization [2, p.3; 4, p.512; 10, p.225]. Also, sea clutter often has a noise-like appearance for vertical polarization and a spiky appearance for horizontal polarization [6, p.2]. An example of this characteristic is shown in Fig. 19. The fact that the polarization dependence of σ° depends upon the sea state or wave height suggests that the polarization dependence is caused by the illumination of the surface by the interference pattern of the radar field.

2.3.3. Variation of σ° with Depression Angle.

For sea water the variation of σ° with depression angle is great near vertical incidence and is much less for small depression angles [13, p. 977; 10, p.224]. The decrease in σ° with depression angle is greater for calm seas than rough seas, as shown in Fig. 2 [7, p.32]. The variation of σ° with depression angle can be 40 db or more as shown in Figs. 9 and 11. From Fig. 11 it can be seen that the clutter is large near normal incidence and drops off sharply to a depression angle of approximately 60°. Below a depression angle of 60° the variation of σ° with angle is less rapid. For horizontal polarization at 220 mc σ° is proportional to Θ^4 for Θ between 1 and 14 degrees [9, p.6]. For vertical polarization at 24.7 mc σ° is about -43 db for small depression angles, which is the same as σ° at 10 kmc [11, p.7].

The measurements also show that the σ° versus depression angle (Θ) curves have a large slope for small values of Θ and a smaller slope at intermediate values of Θ. The angle at which this slope changes is called the critical angle and varies from 1 degree for rough seas to 5 degrees for calm seas [4, p.510].

2.3.4 Variation of σ° with Angle to the Wind.

For sea return, σ° is larger for the upwind heading than the downwind heading, with σ° for the cross wind direction being slightly higher than the downwind value for vertical polarization, and either higher or lower for horizontal polarization [7, p.1]. The upwind-downwind ratio can be as large as 10 db at X band [2, p.3]. For horizontal polarization at 220 mc there is little variation in σ° with azimuth [9, p.6]. A measurement made at higher depression angles revealed that σ° is independent of azimuth from 10 to 35 kmc at a depression angle of 60°.

2.3.5 Variation of σ° with Wind Speed.

For sea clutter, σ° increases with increasing wind speed for angles below vertical incidence from 10 to 50 kmc [4, p.512; 10, p.227]. For wave heights above four feet there is little increase in σ° with wave height. For vertical incidence the trend is usually reversed [10]. For depression angles less than 70°, an increase in wind speed from 5 to 25 knots can increase σ° by more than 20 db in the 15-35 kmc frequency range [13, p.977]. For depression angles below 4°, empirical formulas have been fitted to the measured data at 6.3 and 35 kmc which indicate that σ° varies as $W^{3.2}$ for horizontal polarization and as $W^{2.0}$ for vertical polarization, where W is the wind speed in knots [14, p.85-86].

2.3.6 Clutter Fluctuations.

Sea clutter fluctuations often have a spiky appearance on a radar A-scope indicator. These spikes are more prominent and occur at larger grazing angles for horizontal polarization, and are found at larger pulse widths on L-band than on X-band on horizontal polarization. The spike structure is finer on X-band [6, p.2].

For horizontal polarization at 220 mc, the sea clutter fluctuation-rates are highest for the cross-wind heading. The cross-wind echoes often have twice the period of ocean waves of half the radar wavelength [9, p.6].

For calm seas the doppler spectrum is symmetrical in shape. For rough seas the spectrum is unsymmetrical with the downwind moving scatterers contributing to the broader side of the spectrum [15, p.16]. Doppler shifts of 0.5 cps at 24.7 mc, 0.425 cps at 16.39 mc, and 0.38 cps at 13.5 mc have been measured. Band widths of the spectrum from 2 to 20% have been measured at these high frequencies [5, p.682; 12]. The spectrum at 35 kmc is 5 times as wide as the spectrum at 6.3 kmc [14, p.61].

The sea clutter spectrums show periodic variations due to the large sea waves. The amplitudes of the periods are independent of frequency from 6 to 35 kmc. There is also a fast random fluctuation whose frequency is proportional to the wind speed and radar frequency. There is also a slower random fluctuation which is independent of frequency and larger for horizontal polarisation [14, p.61].

2.4 Comparison of Experimental Results for Ground Return.

Some of the measurement programs mentioned in Sec. 2.2 above have yielded data on ground return. These measurements are compared below for each

parameter. The variation of σ^o with frequency, polarization, depression angle, wind speed and direction, and surface roughness is examined, as well as the measurements of the characteristics of clutter fluctuations.

2.4.1 Variation of σ^o with Frequency.

For ground return the frequency dependence is a function of the type of terrain. For smooth ground such as concrete and asphalt roads, σ^o varies approximately as λ^{-2}, while σ^o varies as λ^{-1} for two-inch-high grass [16]. The results of recent measurements of various types of terrain are shown in Figs. 12 -- 18. Fig. 12 shows that wet marsh lands covered with tall plants have a somewhat unusual frequency characteristic from 3.2 cm to 8.6 mm. That is, the value of σ^o for 3.2 cm lies between the values for 1.25 cm and 8.6 mm. The same effect was noted in a non-homogeneous terrain composed of marshland, sand and bushes as shown in Fig. 13. Figs. 14 -- 16 indicate that terrain covered with trees having foliage, and terrain covered with short or tall dry grass have cross sections which vary approximately as λ^{-1}. Figs. 17 and 18 illustrate the effect of moisture content on the frequency dependence of the ground return. For wet terrain it can be seen that the ground return at 1.25 cm is considerably reduced by the presence of the water, the return for 8.6 mm is increased and the return for 3.2 cm is substantially unchanged for depression angles between 30^o and 80^o, and is increased at the other angles.

2.4.2 Variation of σ^o with Polarization.

For smooth ground σ^o is 5 to 10 db greater for vertical polarization than for horizontal polarization at a depression angle of 20^o, and less than 5 db greater at a depression angle of 80^o at 35 kmc. For rough

ground there is little dependence of σ° on polarization [16].

For a green pasture with 12 to 16 inch high grass, σ° is 2.5 db greater on vertical polarization than horizontal polarization at 9.4 kmc, 1.5 db greater at 16.5 kmc and 1.5 db less at 35 kmc [17].

2.4.3 Variation of σ° with Depression Angle.

For ground return the variation with depression angle depends upon the nature of the terrain. For smooth ground σ° decreases rapidly with depression angle and may decrease as much as 25 db from 80° to 20°, while for rough ground the decrease may be less than 5 db [16]. σ° is much larger at normal incidence for smooth ground than for rough ground. Figs. 12 -- 18 and Figs. 20 -- 24 give typical values for ground return 18. Bare spots in the ground increase σ° at normal incidence, and wet spots increase it even more.

2.4.4 Variation of σ° with Angle to the Wind.

Measurements of the variations of ground clutter with wind direction have not been located.

2.4.5 Variation of σ° with Wind Speed.

Measurements of the variation of ground clutter with wind speed have not been located.

2.4.6 Variation of σ° with Surface Roughness.

For ground return, σ° increases with increasing roughness, and seems to have an upper limit of -3 db to -7 db from 10 to 35 kmc for small depression angles. However, near vertical incidence σ° is larger for smooth surfaces than for rough surfaces [16, p.21].

2.4.7 Clutter Fluctuations.

No doppler measurements for ground return have been located in the unclassified literature.

3.0 SEA CLUTTER THEORIES.

3.1 The Corrugated Surface Theory

One theory which has been proposed for sea clutter is the corrugated surface theory. In this theory the sea is assumed to be made up of long, cylindrical waves with sinusoidal or trochoidal cross sections.

To calculate σ° it is assumed that the surface consists of waves whose amplitudes and lengths both have Gaussian distributions [4, pp.518-521]. The probability density function assumed for the amplitude is

$$p(y) = \frac{y}{A^2} e^{-\frac{y}{2A^2}}, \qquad (3.1)1)$$

where A is the mean amplitude of the waves. The probability density function of the wavelength is assumed to be

$$g(x) = \frac{1}{\sigma_x \sqrt{2\pi}} e^{-\frac{(x-L)^2}{2\sigma_x^2}}, \qquad (3.1.2)$$

where L is the mean length of the waves and σ_x is the standard deviation of the wavelength. For a sinusoidal wave of length y large compared to λ, the energy scattered back to the radar is given by

$$S(\theta) = \frac{E^2}{L}, \qquad (3.1.3)$$

where

$$E = \frac{A}{\sqrt{\lambda}} \sin\theta \, J_\nu(B_y), \qquad (3.1.4)$$

$$\nu = \frac{2x}{\lambda} \cos\theta, \qquad (3.1.5)$$

$$B_y = \frac{4\pi y}{\lambda} \sin\theta, \qquad (3.1.6)$$

and θ is the depression angle. For long low waves σ_x is small compared to L and the result is [4]

$$\sigma^\circ = \frac{L\lambda z^2}{(4\pi A)^2} e^{-z^2} I_m(z^2), \tag{3.1.7}$$

where

$$z = \frac{4\pi A}{\lambda} \sin\theta, \tag{3.1.8}$$

$$m = \frac{2L}{\lambda} \cos\theta, \tag{3.1.9}$$

and I_m is the modified Bessel function of order m. For small depression angles such that

$$\theta < \left(\frac{6L}{\lambda}\right)^{\frac{1}{2}} \frac{\lambda}{4\pi A}, \tag{3.1.10}$$

$$\sigma^\circ = \frac{2\lambda}{(4\pi A)^2} \left(\frac{z^2}{2}\right)^{m+1} \frac{e^{-z^2}}{\Gamma(m+1)}. \tag{3.1.11}$$

For small angles such that

$$\theta \ll \frac{\lambda}{4\pi A}, \tag{3.1.12}$$

$$\sigma^\circ \propto \theta^n, \tag{3.1.13}$$

where

$$n = m+1 = \frac{2L}{\lambda} + 1. \tag{3.1.14}$$

For large angles such that

$$\theta > \frac{L}{2\pi A}, \tag{3.1.15}$$

$$\sigma^\circ = \frac{\sqrt{2L}\,\sin\theta}{(4\pi)^{3/2} A}. \tag{3.1.16}$$

The doppler shift observed for sea clutter has also been described in terms of waves [5]. The waves are assumed to have a sinusoidal shape and a small amplitude. The viscosity of the water is assumed to be zero and the doppler shift is attributed to waves whose lengths are an integral number of half wavelengths at the radar frequency moving radially with respect to the radar. The velocity of a sinusoidal sea wave of length L is

$$v = \sqrt{\frac{gL}{2\pi}}, \tag{3.1.17}$$

where g is the acceleration due to gravity. The doppler shift due to waves of length $L = \frac{n\lambda}{2}$ moving radially toward the radar is

$$\Delta f = \frac{2v}{\lambda} = \sqrt{\frac{gn}{\pi\lambda}}. \qquad (3.1.18)$$

It has been shown that if all directions of wave motion are equally likely, the doppler shifts tend to bunch around the value for radial motion [12, p.18]. This is because the radial component is a cosine function which changes slowly about its maximum near the radial direction, and changes rapidly near the tangential direction.

The corrugated surface theory does explain the observed doppler shifts and the high reflection near normal incidence. However, it does not account for the measured values of clutter obtained at small depression angles and it does not properly account for the critical angle [4, p.522]. This theory does not explain polarization dependence of clutter or the dependence of sea clutter on the angle to the wind.

3.2 The Drop Theory.

One theory which was initially proposed for sea clutter is the Drop Theory [4, p.522-527; 3]. According to the drop theory, the wind causes spray droplets to be thrown into the air. These droplets intercept one or more of the interference lobes and reflect the incident energy back to the radar. For calm seas the drops are not thrown up to large heights and do not reach the first interference lobe so that the return for vertical polarization is stronger than that for horizontal polarization. As the roughness increases, the difference between polarizations decreases.

To calculate σ° the return from drops of a given size at a given height is expressed in terms of the cross section of a single drop, the number of drops per unit area and the interference lobe structure. The drop size dis-

tribution is assumed to be independent of the drop height and an integration is performed over all drop sizes to obtain an average radar cross section per drop. Finally, it is assumed that the distribution of drops with height follows the barometric law, and an integration over all heights is performed to obtain σ°.

The cross section per unit area is given by

$$\sigma^\circ = \int_0^\infty \int_0^\infty \sigma(r)\, n(r, z)\, F^4(z, \theta, \lambda)\, dz\, dr, \qquad (3.2.1)$$

where $F(z,\theta,\lambda)$, the propagation factor which describes the interference lobes, is given by

$$F = 1 + \rho e^{-j(2k\theta z + \phi)}, \qquad (3.2.2)$$

where ρ and ϕ are the amplitude and phase of the reflection coefficient of the sea respectively, $k = \frac{2\pi}{\lambda}$, λ is the radar wavelength, θ is the depression angle, r is the radius of the spray drop, z is the height of the drop above the sea, and $n(r,z)$ is the distribution function of the number of drops per unit area of radius r at a height z.

On the assumption that the distribution of drops in height is independent of the radius,

$$n(r, z) = n_1(r)\, n_2(z), \qquad (3.2.3)$$

and the cross section is

$$\sigma^\circ = N \bar{\sigma} \int_0^\infty n_2(z)\, F^4(z, \theta, \lambda)\, dz, \qquad (3.2.4)$$

where $\bar{\sigma}$ is the average cross section per drop and N is the total number of drops per unit area of the sea. It is assumed that the distribution of drops with height follows the barometric law

$$n_2(z) = \frac{1}{z_0}\, e^{-z/z_0}. \qquad (3.2.5)$$

For horizontal polarization $\rho = 1$, $\phi = \pi$ and equations (3.2.2), (3.2.4) and (3.2.5) give

$$\sigma^\circ = N\bar{\sigma}(2\rho - 1)\frac{24(2k\theta z_0)^4}{1 + 5(2k\theta z_0)^2 + 4(2k\theta z_0)^4} \quad . \qquad (3.2.6)$$

The drop theory provides a qualitative explanation of the polarization of sea clutter, since the interference lobes illuminating the drops are different for the different polarizations. The fact that the drops are thrown up higher to produce more back scattering in higher winds gives a qualitative explanation of the increase in radar cross section with increasing wind speed. The predicted variation of σ° with θ, the depression angle, is also in agreement with the measurements. The drop theory, however, does not properly explain the observed frequency dependence of sea clutter. From equation (3.2.6), a variation proportional to λ^{-4} is obtained for small angles and a variation proportional to λ° for large angles only if the individual drop cross sections are independent of frequency. This would require drops much larger than those observed. The drop theory has not been extended to explain the fluctuations of clutter in terms of the random properties of the size and number distributions.

3.3 The Facet Theory.

This theory assumes that the surface of the sea is composed of many flat facets which scatter the incident energy [19, 20]. The calculation of σ° is divided into two parts, that for small depression angles and that for large angles. For small angles the scattering from small and large circular plates is calculated and these calculations are extrapolated to intermediate sizes. σ° is then calculated from the average value of σ for small and large plates in terms of the number and slope distributions of the facets. For small disks and horizontal polarization the average radar area

is

$$\overline{\sigma_s} = \frac{f_2(\theta) A^3}{\lambda^4}, \tag{3.3.1}$$

where

$$f_2(\theta) = \frac{(4)^5 \left(1 + \cos^2 \frac{\theta}{2}\right)^2}{9} . \tag{3.3.2}$$

The radar area of a large rectangular facet is

$$\sigma = 4\pi \left(\frac{A}{\lambda} \cos\gamma \frac{\sin x}{x} \frac{\sin y}{y} \right)^2, \tag{3.3.3}$$

where

$$x = k W \sin\theta \sin\gamma, \tag{3.3.4a}$$

$$y = k L \cos(\theta + \delta), \tag{3.3.4b}$$

$$\cos\gamma = \cos\beta \sin\theta + \sin\beta \cos\theta \cos\alpha, \tag{3.3.4c}$$

and the angles θ, γ, β, α and δ are defined by Fig. 25. For grazing angles, $\frac{\sin x}{x}$ is unity, and $\sin^2 y$ can be replaced by its average, $\frac{1}{2}$. Putting $W = L$ because the average of all rectangular shapes is a square, the result is

$$\overline{\sigma} = \frac{A z_y^2 (1 + z_y^2)}{2\pi (1 + z_x^2 + z_y^2)} = SA, \tag{3.3.5}$$

where

$$z_x = \tan\gamma \tag{3.3.6a}$$

and

$$z_y = \tan\delta \tag{3.3.6b}$$

are the crosswind and the upwind components of slope, respectively. The radar areas for small circular disks and large square facets have the same value at an area

$$A_1 = \left(\frac{S}{k_2}\right)^{\frac{1}{2}} \lambda^2, \tag{3.3.7}$$

where $k_2 = 2\pi/9$.

The contributions from the facets of varying size and slope are summed by assuming that the phases of the scattered waves are random, so that the

powers can be added directly. It is also assumed that the slope and size distributions are independent. Then, if S is the facet slope,

$$\sigma^\circ = \iint N(A)\,P(s)\,\bar{\sigma}(s,A)\,dA\,ds, \qquad (3.3.8)$$

where $P(s)$ is the probability density of facet slopes, and $N(A)$ is the number density of facet sizes. Since experiments have shown that σ° is proportional to λ^{-n}, $N(A)$ is assumed to be of the form

$$N(A) = N_0 A^{-m}, \qquad (3.3.9)$$

where N_0 is a constant. If $N(A)$ is small for the largest and smallest facet areas, the limits of integration can be extended to zero and infinity and

$$\int N(A)\,\bar{\sigma}\,dA = N_0\left[\int_0^{A_1} k_2 \lambda^{-n} A^{3-m}\,dA + \int_{A_1}^{\infty} S A^{1-m}\,dA\right]. \qquad (3.3.10)$$

Applying equation (3.3.7) and letting $n = 2m-4$ gives

$$\int N(A)\,\bar{\sigma}\,dA = \frac{8 N_0 k^{n/4} \lambda^{-n}}{n(4-n)} S^{\frac{4-n}{4}} \qquad (3.3.11)$$

and

$$\sigma^\circ = \frac{8 N_0 k_2^{n/4} \lambda^{-n}}{n(4-n)} \int_0^{\infty}\int_{-\infty}^{\infty} P(z_x, z_y)\, S^{1-n/4}\,dz_x\,dz_y. \qquad (3.3.12)$$

Then, use is made of the experimentally determined probability density distribution [25]

$$P(z_x, z_y) = (2\pi\sigma_c\sigma_u)^{-1} e^{-\frac{1}{2}(\xi^2+\eta^2)}\left\{1 - \frac{c_{21}}{2}(\xi^2-1)\eta\right. \qquad (3.3.13)$$
$$\left. - \frac{c_{03}}{6}(\eta^3-3\eta) + \frac{c_{40}}{24}(\xi^4-6\xi^2+3) + \frac{c_{22}}{4}(\xi^2-1)(\eta^2-1) + \frac{c_{04}}{24}(\eta^4-6\eta^2+3)\right\}$$

where $\sigma_c^2 = 1.15(10)^{-3}W$, $\sigma_u^2 = 1.65(10)^{-3}W$, $c_{21} = -0.003W$, $c_{03} = -0.015W$, $c_{40} = 0.4$, $c_{22} = 0.12$, $c_{04} = 0.23$, W is the wind speed in knots, $\xi = z_x/\sigma_c$, $\eta = z_y/\sigma_u$ and σ_c and σ_u are the RMS values of z_x and z_y respectively.

Then letting $n = 1$ gives

$$\sigma^\circ \approx 9(10)^{-3} N_0 \lambda^{-1} W^{3/4}\left[1 \pm 2(10)^{-3} W\right], \qquad (3.3.14)$$

where W is positive for the upwind direction. The upwind-to-downwind ratio

is

$$\frac{\sigma_u^\circ}{\sigma_d^\circ} = \frac{1+2(10)^{-3}W}{1-2(10)^{-3}W} \quad . \tag{3.3.15}$$

For large grazing angles the large facets will scatter more energy back to the radar, since some of these are viewed broadside. The radar area of a large flat plate at normal incidence will be $\sigma = \frac{4\pi A^2}{\lambda^2}$, where A is the area of the plate. However, the plate will have a solid angle beamwidth proportional to λ^2/A, so that the overlapping of patterns of facets of different slopes will decrease as the facet size increases. This compensates for the increasing value of facet area with size so that the smaller facets are equally significant contributors to the total radar area.

The calculations of σ° for large depression angles assumes that the phases of the scattered waves are random so that the powers may be added directly. Also it assumes that multiple reflections can be neglected for $45^\circ < \theta < 90^\circ$, since it is very improbable that there will be wave slopes greater than 40°. For small facets at large depression angles we have, from equations (3.3.1) and (3.3.2), an average value independent of depression angle given by

$$\sigma_s^\circ = \frac{2^{10}}{9}\left(\frac{A}{\lambda^2}\right)^2, \tag{3.3.16}$$

and for large facets

$$\sigma_l^\circ = \frac{4\pi A}{\lambda^2} \quad . \tag{3.3.17}$$

These facets have the same radar cross section for an area

$$A = A_1 = 0.1104\,\lambda^2. \tag{3.3.18}$$

The geometry of Fig. 26 is used, where the line OP is the line of steepest ascent on the facet, and the direction cosines of the wave normal with respect to the facet axes x', y', z' are l, μ, ν respectively. With this notation the radar area of a large rectangular facet is

$$\sigma = \frac{1}{\pi}\left(k A_y \frac{\sin Bl}{Bl} \frac{\sin Cw}{Cw}\right), \qquad (3.3.19)$$

where $B = \frac{2\pi w}{\lambda}$, $C = \frac{2\pi L}{\lambda}$ and w and L are the width and length of the facet respectively. If all of the facet orientations are equally probable the average cross section for large facets will be

$$\bar{\sigma} = \frac{1}{2\pi}\int_0^{2\pi} \sigma\, dw = 2\left(\frac{A\nu}{\lambda}\right)^2 \int_0^{2\pi}\left(\frac{\sin Bl}{Bl} \frac{\sin Cw}{Cw}\right)^2 dw. \qquad (3.3.20)$$

Since the square is the average of all rectangular shapes, this can be reduced to

$$\bar{\sigma} = 4\pi\left(\frac{A\nu}{\lambda}\right)^2 \sum_{n=0}^{\infty} (b_n B)^{2n}, \qquad (3.3.21)$$

where

$$B^2 = (kw)^2(1-\nu^2), \qquad (3.3.22)$$

and the b_n's are tabulated in the literature [10]. The summation is plotted in Fig. 27. Now substituting equations (3.3.13) and (3.3.21) into equation (3.3.8) gives

$$\sigma_\ell^\circ = \int_{A_1}^{A_2} N(A)\, dA \int_0^{\pi/2} d\beta \int_0^{2\pi} P(\alpha,\beta)\,\bar{\sigma}\, d\omega. \qquad (3.3.23)$$

Approximating some of the resulting integrals by their asymptotic expansions leads to

$$\sigma_\ell^\circ = \frac{1}{2\pi\sigma_c\sigma_u} \int_{A_1}^{A_2} N(A) \sum_{n=0}^{\infty} \left(\frac{c}{2}\right)^n \left[E_{n0} + E_{n1} + \sum_{m=2}^{\infty} E_{nm} \frac{(n+m-2)!}{n!\, q^{n+m-1}}\right] dA \qquad (3.3.24)$$

where $0.11 < q < 0.11 + \frac{300}{A_1}$ and the E_{nm} involve θ and A. If it is assumed that

$$N(A) = N_0 A^{-m}, \qquad (3.3.9)$$

then it is possible to solve equation (3.3.24) for σ° as a function of the various parameters. If the facets are oriented with the wind, a more compact form can be obtained for σ_ℓ°. For this case we have the geometry of Fig. 23 and

$$\sigma_\ell^\circ = \frac{k^2}{\pi} \int_{A_1}^{A_2} A^2 N(A)\, dA \int_{-\infty}^{\infty}\int_{-\infty}^{\infty} \nu^2 P(\xi_x, \xi_y) \frac{\sin^2 Bl}{Bl} \frac{\sin^2 Cw}{Cw}\, d\xi_x\, d\xi_y, \qquad (3.3.25)$$

which, if we assume the square as an average of all rectangular shapes, gives

$$\sigma_f^\circ = \frac{4\pi}{\lambda^2}\int_{A_1}^{A_2} G A^2 N(A)\,dA\,, \qquad (3.3.26)$$

where

$$G = \frac{\pi}{2\sigma_c\sigma_u k^2 A}\, e^{-\frac{\cot^2\theta}{2\sigma_u^2}} \left\{ \ldots \right\}. \qquad (3.3.27)$$

For small facets the scattering is assumed to be independent of slope so that

$$\iint P\,d\zeta_x\,d\zeta_y = 1, \qquad (3.3.28)$$

and from equation (3.3.1)

$$\sigma_s^\circ = \frac{2^{10}}{9\lambda^4}\int_{A_0}^{A_1} A^3 N(A)\,dA, \qquad (3.3.29)$$

which leads to

$$\sigma^\circ = \sigma_s^\circ + \sigma_f^\circ = 2N_0\Big[\lambda^{-n}\Big(\frac{g_0}{4-n}a_0^{\frac{4-n}{2}} + \frac{g_1}{n}a_0^{-\frac{n}{2}} + \frac{g_2}{n+1}a_0^{-\frac{(n+1)}{2}}\Big) - \Big(\frac{g_0}{4-n}\lambda^{-4}A_0^{\frac{4-n}{2}} + \frac{g_1}{n}A_2^{-\frac{n}{2}} + \frac{g_2}{n+1}A_2^{-\frac{(n+1)}{2}}\Big)\Big], \qquad (3.3.30)$$

where

$$g_0 = \frac{2^{10}}{9}, \qquad (3.3.31a)$$

$$g_1 = \frac{e^{-\frac{\cot^2\theta}{2\sigma_u^2}}}{2\sigma_c\sigma_u}\Big[1 + \frac{c_{40}}{8} + \frac{c_{22}}{4}(1-\cot^2\theta) - \frac{c_{04}}{3}(3-\cot^2\theta) + \frac{c_{04}}{24}(1+\sigma_u^2\cot^4\theta)(3-6\cot^2\theta+\cot^4\theta) + \frac{c_{13}\sigma_u\cot^3\theta}{2}\Big], \qquad (3.3.31b)$$

$$g_2 = \frac{e^{-\frac{\cot^2\theta}{2\sigma_u^2}}}{2K\sigma_u}\Big[\frac{c_{40}}{12}(\sigma_c^2-6) - \frac{c_{22}}{12}(1-\cot^2\theta) - c_{13}\sigma_u\cot^3\theta\Big] - \frac{g_1}{K\sigma_c}, \qquad (3.3.31c)$$

$$K = (2\pi)^{3/2}\sin\theta\,. \qquad (3.3.31d)$$

The facet theory predicts an approximately Gaussian variation of σ° with depression angle near normal incidence, and no variation with angle at grazing incidence, which agrees with the experimental data. The correct frequency dependence is included in the $n = 1$ assumption. The polarisation dependence is explained qualitatively by the illumination of the facets by the interference lobes. The variation of radar area with angle to the wind is

also explained, although the predicted upwind-to-downwind ratio is much smaller than the measured value. This theory gives a variation of σ° proportional to the wind speed to the 3/4-power for small depression angles, and inversely proportional to the wind speed at large angles. This dependence is in good agreement with the existing experimental data. The facet theory has not been extended to explain the fluctuations of clutter in terms of the random properties of the facet slopes.

4.0 GROUND CLUTTER THEORIES.

4.1 Slightly Rough Surfaces.

One theory of ground clutter considers the surface of the earth to be almost smooth (or only slightly rough) [21, 22]. The variations of the height of the surface above a plane are assumed to be random and the roughness is described by a roughness distribution function which is an average over an ensemble of similar surfaces. It is assumed that the average distance between hills is large and that the surface is smooth except for these hills, so that the slope of the surface is small everywhere. The scattered field is assumed to consist of a series of plane waves. The back-scattered power from an elemental area of the surface is determined neglecting higher order boundary conditions, and the radar cross section is determined by integrating over the entire surface.

The altitude of a point (x,y) in a large square of side L can be expressed as

$$z = f(x,y) = \sum_{-\infty}^{\infty} \sum_{-\infty}^{\infty} P(m,n)\, e^{-j\alpha(mx+ny)} , \qquad (4.1.1)$$

where m and n are integers and $\alpha = 2\pi/L$. Since z is real,

$$P(m,n) = P^*(-m,-n) . \qquad (4.1.2)$$

Since the surface is assumed to be random, an average over an infinite number of areas of side L gives

$$\langle P(m,n)\rangle = 0. \tag{4.1.3}$$

The roughness distribution function is given by

$$W(p,q) = \left(\frac{L}{\pi}\right)^2 \langle P(m,n)\,P^*(m,n)\rangle \tag{4.1.4}$$

where $p = 2\pi m/L$ and $q = 2\pi n/L$. Since the Fourier coefficients are independent,

$$\langle P(m,n)\,P(u,v)\rangle = 0, \quad (u,v) \neq (-m,-n). \tag{4.1.5}$$

For horisontal polarisation the horizontal reflected component for a perfect conductor is a summation of plane waves which can be written as

$$E_y = 2j \sin(kz \sin\theta_s)\, e^{-jkx\cos\theta_s} + \sum B_{mn} E(m,n,z) \tag{4.1.6}$$

where

$$E(m,n,z) = e^{-j[a(mx+ny) - b(m,n,z)]}, \tag{4.1.7}$$

$$b(m,n) = [a^2(m^2+n^2) - k^2]^{\frac{1}{2}}, \tag{4.1.8}$$

$$a_m = k \sin\theta_s \cos\phi_s, \tag{4.1.9a}$$

$$a_n = k \sin\theta_s \sin\phi_s, \tag{4.1.9b}$$

and θ_s and ϕ_s are the elevation and azimuth angles of the scattered ray respectively.

The power P_s scattered into a unit solid angle in the direction (θ_s, ϕ_s) is

$$\frac{P_s}{\cos^2\phi_s} = |B_{mn} E(m,n,z)|^2 \frac{dm\,dn}{d\Omega} = \left(\frac{k}{a}\right)^2 \cos\theta_s |B_{mn}|^2, \tag{4.1.10}$$

where

$$d\Omega = \sin\theta_s\, d\theta_s\, d\phi_s. \tag{4.1.11}$$

The value of B_{mn} is found from the boundary conditions (neglecting high order terms) to be

$$B_{mn} = -2jk\sin\theta\, P(m-\nu, n), \tag{4.1.12}$$

where

$$\nu = \frac{k}{a}\cos\theta, \tag{4.1.13}$$

the slope of the surface is small everywhere and the boundary is assumed to be a perfect conductor. The radar cross section then becomes

$$\sigma^\circ = 4\pi P_s T = \left[4\pi k^4 \sin^2\theta \cos\theta_s W(am-a\nu, an)\cos^2\phi_s\right] T \tag{4.1.14}$$

where T, the factor included for dielectric surfaces, is given for horizontal and vertical polarization respectively by

$$T_h = \left| \frac{\varepsilon_c - 1}{\left[\sin\theta - (\varepsilon_c - \cos^2\theta)^{\frac{1}{2}}\right]^2} \right|^2, \tag{4.1.15a}$$

$$T_v = \left| \frac{(\varepsilon_c - 1)\left[\cos^2\theta(\varepsilon_c - 1) + \varepsilon_c\right]}{\left[\varepsilon_c \sin\theta + (\varepsilon_c - \cos^2\theta)^{\frac{1}{2}}\right]^2} \right|^2. \tag{4.1.15b}$$

The radar cross section in terms of the height correlation function $\rho(r)$ is given by

$$\sigma^\circ = 8\sin^3\theta\, \overline{z^2} k^4 T \int_0^\infty J_0(2kr\cos\theta)\rho(r) r\, dr, \tag{4.1.16}$$

where it is assumed that the surface is isotropic and is given by

$$\overline{z^2} = \lim_{L\to\infty} \frac{1}{L^2} \int_{-\frac{L}{2}}^{\frac{L}{2}} \int_{-\frac{L}{2}}^{\frac{L}{2}} f^2(x, y)\, dx\, dy, \tag{4.1.17}$$

and

$$\rho(r) = \lim_{L\to\infty} \frac{1}{L^2} \int_{-\frac{L}{2}}^{\frac{L}{2}} \int_{-\frac{L}{2}}^{\frac{L}{2}} \frac{f(\xi, \eta) f(\xi + x, \eta + y)}{\overline{z^2}}\, d\xi\, d\eta. \tag{4.1.18}$$

This theory accounts for the polarization dependence with the T functions of equations (4.1.15a) and (4.1.15b). The theory also explains the variation of σ° with depression angle reasonably well for smooth surfaces such as concrete and asphalt roads if the proper ground constants are chosen. However, more information is needed about the electrical properties of the various terrains encountered. The variation of σ° with surface roughness is also explained for relatively smooth surfaces. From equation (4.1.13)

the variation of σ° is proportional to λ^{-4} regardless of incidence angle, which explains the measurements at small depression angles but not those at large angles. The theory does not include variations in σ° with wind speed or angle and has not been extended to describe the observed clutter fluctuations.

4.2 Thin Lossy Cylinders.

An attempt has been made to describe the scattering from certain types of ground (tall grass, for example) by considering the ground to be composed of many thin lossy cylinders [21]. It is assumed that these cylinders are distributed over the surface with a prescribed probability distribution for the orientations of the axes. It is assumed that the diameters of the cylinders are less than a wavelength and that the cylinders are sufficiently long and lossy to prevent reflection from the underlying ground. It is assumed that the attenuation is exponential with depth and is due to the resistivity of the cylinders. In other words the attenuation due to scattering is neglected.

To calculate σ°, it is assumed that the surface consists of an array of cylinders. The incident field on a single cylinder is calculated and resolved into components, parallel and normal to the cylinder axis. The boundary conditions are then applied to find the field and current distributions in the cylinder. The horizontal component of the field scattered from a single cylinder is determined, and these components are summed over all cylinders to give the radar cross section.

Consider a single cylinder whose orientation is specified by the unit vector $\hat{n}$ in the x, ψ direction. For horizontal polarization, the incident field is

$$\vec{E}_t = \vec{x}_0 E_0 e^{jk(y\cos\theta - z\sin\theta)} e^{\alpha t}, \qquad (4.2.1)$$

where the projection of the cylinder on the z axis is limited to $z \leq 0$, E_0 is the amplitude and α is the attenuation constant.

The total field is resolved into components parallel and perpendicular to the cylinder axis and the fields inside and outside the cylinder matched using boundary conditions. For boundary conditions it is assumed that the tangential component of E is continuous and the ratio of the normal components of E is $2/(1+\varepsilon_1)$ where ε_1 is the dielectric constant of the cylinder. Thus the field in the conductor is

$$\vec{E}_c = (\vec{E}_t \cdot \vec{n})\vec{n} + \left(\frac{2}{1+\varepsilon_1}\right)\left[\vec{E}_t - (\vec{E}_t \cdot \vec{n})\vec{n}\right], \qquad (4.2.2)$$

the current distribution is

$$\vec{J}_c = \left[\sigma - j\omega\varepsilon_0(\varepsilon_1 - 1)\right]\vec{E}_c, \qquad (4.2.3)$$

and the horizontal component of the scattered field is

$$E_x^s = \frac{j\omega\mu}{4\pi R} e^{jkR} \int \vec{J}_c \cdot \vec{x}\, e^{jk\vec{p}\cdot\vec{R}_1}\, dV \qquad (4.2.4)$$

where R is the distance between the radar and the cylinder, $\vec{R}_1$ is a unit vector in the scattering direction and $\vec{p}$ specifies the position of the element dV. If the cylinder diameter is less than the wavelength and the cross-sectional area is A, $dV = a\,ds$ and $\vec{p} = s\vec{n}$ where s is the cylinder length. Since the incident wave is completely attenuated by the cylinders, the integral can be extended to $-\infty$ and

$$\frac{E_x^s}{E_0} = \frac{k^2 A e^{jkR}}{4\pi R} \cdot \frac{\left[(\varepsilon_1 - 1) + j\varepsilon_2\right]\left[\cos^2\chi + \frac{2}{1+\varepsilon_1}\sin^2\chi\right]}{\left[\alpha\sin\chi\cos\psi + 2jk\sin\chi\sin(\theta - \psi)\right]}. \qquad (4.2.5)$$

The radar area is given by

$$\sigma^0 = 4\pi P(s), \qquad (4.2.6)$$

where $P(s)$ is the square of the amplitude of E_x/E_0 multiplied by the number of cylinders per unit area and averaged over the angular distribution

of cylinders, using the weighting function $\sin x \cos\psi$. This gives

$$\sigma^{\circ}_{h} = \frac{NA^2k^2}{4\pi} \cdot \frac{\left[\frac{(\varepsilon_1-1)^2+\varepsilon_2^2}{35}\right]\left[3+\frac{16}{1+\varepsilon_1}+\frac{96}{(1+\varepsilon_1)^2}\right]}{\frac{3}{5}(\alpha_h/k)^2+\frac{4}{5}(1+2\sin^2\theta)}, \qquad (4.2.7a)$$

$$\sigma^{\circ}_{v} = \frac{NA^2k^2}{4\pi} \cdot \frac{\left[\frac{(\varepsilon_1-1)^2+\varepsilon_2^2}{35}\right]\left[12+\frac{8}{1+\varepsilon_1}-\frac{64}{(1+\varepsilon_1)^2}\right]\cos^2\theta+\left[3+\frac{16}{1+\varepsilon_1}+\frac{96}{(1+\varepsilon_1)^2}\right]}{\frac{3}{5}(\alpha_v/k)^2+\frac{4}{5}(1+2\sin^2\theta)}, \qquad (4.2.7b)$$

where

$$\alpha_h = \frac{3}{8}(AN\varepsilon_2)\csc\theta\left[1+\frac{12}{(1+\varepsilon_1)^2}\right], \qquad (4.2.8a)$$

$$\alpha_v = \frac{3}{8}(AN\varepsilon_2)\csc\theta\left\{1+\frac{12}{(1+\varepsilon_1)^2}+\cos^2\theta\left[1-\frac{4}{(1+\varepsilon_1)^2}\right]\right\}. \qquad (4.2.8b)$$

A is the cross sectional area of the cylinder, N is the number of cylinders per unit area, $\varepsilon_1 + j\varepsilon_2$ is the complex dielectric constant and $\frac{1}{\alpha}$ is the depth at which the incident field is reduced to $\frac{1}{e}$ times its value at the surface.

This theory agrees roughly with the measured λ^{-1} dependence of σ° on frequency from some specific types of terrain if the constants involving the electrical characteristics of the ground are properly selected. The polarization dependence is explained by the attenuation function of equations (4.2.8). The variation of σ° with depression angle is reasonably well described for properly chosen ground constants. More information is required on the actual constants for various types of terrain. The theory does not explain the variation of σ° with wind speed or direction. The theory does not explain the effect of surface roughness because it is based upon the assumption that the tops of all cylinders lie in a horizontal plane. The theory has not been developed to describe the observed clutter fluctuations.

5.0 MISCELLANEOUS MODELS FOR GROUND RETURN.

Several models have been suggested to partially explain the reflections

which occur from particular types of terrain. Since these are referred to occasionally in the literature, they are included here for completeness. These models assume the surface either has simple statistical properties or consists of arrays of objects of simple shape.

5.1 Optically Rough Surface Described by Lambert's Law.

Often, for rough surfaces the reflected light can be described by Lambert's Law [23], the reflected waves being given by

$$P' = K \sin\theta , \tag{5.1.1}$$

where K is a constant and θ is the grazing angle. If S_o is the power density in the incident wave, the incident power on an area A is

$$P_i = S_o A \sin\theta , \tag{5.1.2}$$

and the reflected power density at unit distance is

$$S_r = \frac{S_o A}{4\pi} K \sin^2\theta , \tag{5.1.3}$$

so that

$$\sigma = KA \sin^2\theta , \tag{5.1.4}$$

and the normalized radar cross section is

$$\sigma^o = K \sin^2\theta . \tag{5.1.5}$$

The only frequency and polarization dependence is that given by the reflection coefficient, and the depression angle dependence of $\sin^2\theta$ does not agree with measurements made at small angles. The theory does not explain the effects of wind or surface roughness and cannot describe the fluctuations which exist.

5.2 Two Dimensional Array of Spheres.

This model considers the ground to be made up of a two dimensional

array of spheres which reradiate equally in all directions, are independent of the incident angle and are randomly distributed in height so that the reflected powers can be added algebraically [23].

The power incident on an area A containing N spheres per unit area all having a cross-sectional area A_k will be

$$P_i = S_o A_k N A \,. \tag{5.2.1}$$

Since each sphere reradiates isotropically, the reflected power density at unit distance is

$$S_r = \frac{S_o A_k N A}{4\pi} \,, \tag{5.1.2}$$

so that the radar area is

$$\sigma = A_k N A \,, \tag{5.2.3}$$

and

$$\sigma^o = A_k N = \text{Constant}. \tag{5.2.4}$$

This theory gives a value of σ^o which is independent of frequency and fits certain types of rough terrain. However, it predicts a radar return which is independent of polarization, depression angle, wind and surface roughness, and therefore does not explain the measured results; it also does not explain observed clutter fluctuations.

5.3 Three Dimensional Array of Spheres.

This model considers the ground to be made up of a three dimensional array of spheres separated almost equally in all directions [23]. The spheres are randomly placed so that their reflected powers can be added algebraically. The power incident in an area A will be

$$P_i = S_o A \sin\theta \,, \tag{5.3.1}$$

where S_o is the incident power density and θ is the depression angle. If

each sphere reflects a fraction δ of the power incident upon it, all spheres are identical, there are no multiple reflections, and the layer of spheres is sufficiently thick so that all of the power is reflected. The reflected power will be

$$P_r = \delta P_i = \delta S_0 A \sin\theta, \qquad (5.3.2)$$

so that the radar area is

$$\sigma = \delta A \sin\theta, \qquad (5.3.3)$$

and

$$\sigma^\circ = \delta \sin\theta. \qquad (5.3.4)$$

Therefore σ° is proportional to the projected area of the ground normal to the axis of the illuminating radar beam.

The only frequency and polarisation dependence is that given by the reflection coefficient. The variation with depression angle of $\sin\theta$ describes certain types of terrain. However the theory predicts a radar return which is independent of wind and surface roughness and the observed fluctuations are not explained.

5.4 Independent Random Scatterers.

This model considers the ground to consist of a non-reflecting surface upon which is distributed a large number of random scatterers [24]. For short wavelengths these scatterers are independent, while for long wavelengths neighboring elements scatter coherently. Assumptions are made regarding the density of these scatterers and their area, and from these assumptions a value for the radar cross section is computed.

If P_s is the average number of scatterers per unit area and A_s is the average area of these scatterers, then the radar cross section per unit area is

$$\sigma^{\circ} = \frac{4\pi \rho P_s A_s}{\lambda^2} , \qquad (5.4.1)$$

where ρ is the reflection coefficient and λ is the wavelength. If the density of the scatterers is independent of wavelength at short wavelengths, and is proportional to λ^{-2} for large wavelengths where neighboring elements scatter coherently, then the density of effective scatterers is given by

$$P_s = P_o \qquad \lambda \leq \sqrt{\frac{c}{P_o}} , \qquad (5.4.2)$$

$$P_s = \frac{c}{\lambda^2} \qquad \lambda \geq \sqrt{\frac{c}{P_o}} , \qquad (5.4.3)$$

where C is a constant of order unity. Then if it is assumed that for small wavelengths the effective area of a scatterer is equal to the geometric area and for long wavelengths the effective area is that of an isotropic scatterer (one having unit gain), the effective area will be $\lambda^2/4\pi$. These areas are equal for a wavelength

$$\lambda_1 = \sqrt{4\pi A_g} , \qquad (5.4.4)$$

where A_g is a geometrical area of the scatterer. Combining the two values of scatterer density and scatterer area gives the following four values for radar cross section:

	$\lambda \leq \sqrt{4\pi A_g}$	$\lambda \geq \sqrt{4\pi A_g}$
$\lambda \leq \sqrt{\frac{c}{P_o}}$	$\sigma^{\circ} = \frac{4\pi \rho P_o A_g^2}{\lambda^2}$	$\sigma^{\circ} = \frac{\rho P_o \lambda^2}{4\pi}$
$\lambda \geq \sqrt{\frac{c}{P_o}}$	$\sigma^{\circ} = \frac{4\pi \rho c A_g^2}{\lambda^4}$	$\sigma^{\circ} = \frac{\rho c}{4\pi}$

This model gives a frequency dependence which varies from λ^2 to λ^{-4}. The variation with polarization is given by the reflection coefficient, but there is no variation with depression angle and no dependence upon external factors such as the wind. The radar area predicted by this model depends upon constants (C, P_o) which have not yet been evaluated. This evaluation pro-

sumably would be accomplished by fitting the theory to measured data.

5.5 Two Dimensional Gaussian Slope Model.

This model assumes the surface has a Gaussian Slope distribution in both dimensions, and assures the radar return is due to the facets aligned perpendicular to the incident wave [24]. The radar area is expressed in terms of the density of the scatterers and their average area, and expressions for these values are found from the statistics of the surface.

If P_s is the average number of scatterers per unit area and A_s is the average area of these scatterers, the radar cross section per unit area is given by

$$\sigma^\circ = \frac{4\pi\rho P_s A_s}{\lambda^2}, \tag{5.5.1}$$

The probability density of the surface slope is

$$p(z_x, z_y)\,dz_x\,dz_y, \tag{5.5.2}$$

where $z(x,y)$ is the height and z_x and z_y are the derivatives of z with respect to x and y respectively. If the slopes necessary to have the facets reflect are

$$\begin{aligned} z_x &= \alpha(x,y), \\ z_y &= \beta(x,y), \end{aligned} \tag{5.5.3}$$

then the probability density of these slopes is

$$p_1(\alpha,\beta)\,|z_{xx}z_{yy} - z_{xy}^2|\,dx\,dy. \tag{5.5.4}$$

If the second derivatives are statistically independent of the first derivatives, then the probability that a reflecting point exists in the area $dx\,dy$ is

$$P_s = \langle |z_{xx}z_{yy} - z_{xy}^2| \rangle p_1(\alpha,\beta). \tag{5.5.5}$$

If the slopes are normally distributed about zero with equal variances and are

statistically independent then

$$P_s = P_s(90°)\, e^{-\frac{c\rho^2 \ell^2 \theta}{2\sigma_{s\theta}^2}} \quad . \qquad (5.5.6)$$

Now if $\sigma_{s\theta}$ is the rms slope on the surface, the density of scatterers will be a constant for short wavelengths and will be inversely proportional to the wavelength at large wavelengths, giving

$$P_s(90°) = \frac{C}{\lambda_1^2} \qquad \lambda \le \lambda_1 , \qquad (5.5.7a)$$

$$P_s(90°) = \frac{C}{\lambda^2} \qquad \lambda \ge \lambda_1 , \qquad (5.5.7b)$$

where C is an arbitrary constant. This model assumes that the effective area of a scatterer is equal to the geometric area (A_g) for short wavelengths and is equal to the area of an isotropic scatterer ($\lambda^2/4\pi$) for long wavelengths. The wavelength at which these areas are equal is given by

$$\lambda_1 = \sqrt{4\pi A_g} \quad . \qquad (5.5.8)$$

combining equations (5.5.6), (5.5.7), and (5.5.8) gives the radar cross section as

$$\sigma^\circ = \frac{4\pi c A_g^2 \rho}{\lambda^2 \lambda_1^2}\, e^{-\frac{c\rho^2 \ell^2 \theta}{2\sigma_{s\theta}^2}} \qquad \lambda \le \lambda_1 , \qquad (5.5.9a)$$

$$\sigma^\circ = \frac{c\rho}{4\pi}\, e^{-\frac{c\rho^2 \ell^2 \theta(\lambda_1)}{2\sigma_{s\theta}^2}} \qquad \lambda \ge \lambda_1 . \qquad (5.5.9b)$$

This theory has not yet been applied to measured results in detail either to evaluate the constants or to determine the success with which this theory describes the measurements. The calculated radar cross section is a function of frequency, polarization (reflection coefficient), depression angle and surface roughness.

5.6 Slightly Rough and Very Rough Surfaces.

This model makes use of an assumed autocorrelation function of the height of points on the surface to calculate the scattered field for the cases

of a very smooth and a very rough surface [26].

The field at a distance r in a direction (θ, ϕ) from a plane wave of amplitude ρ obliquely incident at an angle ψ on a rectangular reflector of dimensions ℓ and m (with ℓ parallel to the plane of incidence) is

$$E = \int_{-\ell/2}^{\ell/2} \int_{-m/2}^{m/2} \frac{\rho}{2\lambda r} [\cos\theta + \cos\psi] \exp\left\{\frac{2\pi i}{\lambda}[x(\sin\theta\cos\phi - \sin\psi) + y\sin\theta\sin\phi + z(\cos\theta + \cos\psi)]\right\} dx\,dy.$$

For a perfectly smooth surface $z = 0$ and E is of the form

$$E = E_0 \left(\frac{\sin A\ell}{A\ell}\right)\left(\frac{\sin Bm}{Bm}\right). \qquad (5.6.2)$$

Now, it is assumed that the distribution in height is Gaussian, so that

$$P(z) = \frac{1}{\sigma\sqrt{2\pi}} \exp\left(-\frac{z^2}{2\sigma^2}\right), \qquad (5.6.3)$$

which gives

$$\langle \exp\left[\frac{2\pi i z}{\lambda}(\cos\theta + \cos\psi)\right]\rangle = \exp\left[-\frac{2\pi^2\sigma^2}{\lambda^2}(\cos\theta + \cos\psi)^2\right] \qquad (5.6.4)$$

and

$$\langle E\rangle = E_0 \left(\frac{\sin A\ell}{A\ell}\right)\left(\frac{\sin Bm}{Bm}\right) \exp\left[-\frac{2\pi^2\sigma^2}{\lambda^2}(\cos\theta + \cos\psi)^2\right] \qquad (5.6.5)$$

which is the usual reflection formula modified by an exponential term.

For the case of a slightly rough surface, $\sigma \ll \lambda$ and $z \ll \lambda$. For a statistical description of the surface, it is assumed that the autocorrelation function of the height of the surface is given by

$$\langle z(x, y), z(x', y')\rangle = \sigma^2 \exp\left\{-\frac{1}{a^2}[(x - x')^2 + (y - y')^2]\right\}, \qquad (5.6.6)$$

where $x' = x + s$ and $y' = y + t$. Since the surface is almost smooth, $\ell >> a$, $m >> a$ and the limits of integration for s and t may be extended to infinity to give

$$\langle |E - \langle E\rangle|^2\rangle = \frac{\pi^3 \rho^2 a^2 \sigma^2 \ell m}{\lambda^4 r^2} (\cos\theta + \cos\psi)^4 \exp\left\{-\frac{\pi^2 a^2}{\lambda^2} \cdot [(\sin\theta\cos\phi - \sin\psi)^2 + \sin^2\theta\sin^2\phi]\right\} \qquad (5.6.7)$$

Now, since

$$\langle|E|^2\rangle = \langle E\rangle^2 + \langle|E-\langle E\rangle|^2\rangle \,, \qquad (5.6.8)$$

the reflected wave can be considered to consist of a coherent and an incoherent component. Both components are concentrated in a cone with an angle determined by the ratio a/λ. If this angle is small

$$\langle|E-\langle E\rangle|^2\rangle = \frac{16\pi^3 e^2 a^2 \sigma \ell m}{\lambda^4 r^2} \cos^4\psi \exp\left[-\frac{\pi^2 a^2}{\lambda^2}(\chi^2\cos^2\psi + w^2)\right] \qquad (5.6.9)$$

$$\chi = \theta - \psi \,, \quad w = \phi \sin\psi$$

For the case of a very rough surface $\sigma >> \lambda$. It is assumed that the surface slope is small so that there is no shadowing. It is then assumed that the probability distribution in height at a distance r from a given surface point z_0 is centered about z_0 for r small, is centered about $z = 0$ for r large, and is expressed as

$$P(z, z_0, r) = \frac{1}{\sigma\sqrt{2\pi}\left[1-\exp\left(-\frac{2r^2}{a^2}\right)\right]^{\frac{1}{2}}} \exp\left\{\frac{-\left[z - z_0 \exp\left(-\frac{r^2}{a^2}\right)\right]^2}{2\sigma^2\left[1-\exp\left(-\frac{2r^2}{a^2}\right)\right]}\right\}. \qquad (5.6.10)$$

This has the same autocorrelation function as that given in Equation (5.6.6) for the slightly rough surface and leads to

$$\langle|E-\langle E\rangle|^2\rangle = \frac{a^2 e^2 \ell m}{8\pi^2\sigma^2 r^2}\cos^2\psi \exp\left[-\frac{a^2}{8\sigma^2}(\chi^2 + w^2\sec^2\psi)\right], \qquad (5.6.11)$$

if we assume, as before, that the radiation is confined to a small cone about the direction of specular reflection.

For the case of back scattering the incident power is

$$P_i = \frac{P_t G_t}{4\pi R^2} \,, \qquad (5.6.12)$$

and the reflected field at the transmitter is

$$E_r = \iint \frac{(P_i)^{\frac{1}{2}}}{\lambda R}\cos\psi \exp\left(\frac{j4\pi r}{\lambda}\right) dx\, dy, \qquad (5.6.13)$$

where P_t and G_t are the transmitter power and gain respectively. Now, if the antenna pattern is uniform and confined to a small azimuth angle β and a small elevation angle ψ, and it is assumed that variations in range,

R, affect only the phase, then the statistical description of the surface given by Equation (5.6.10) for a rough surface gives

$$P_r = \frac{P_t G A a^2 \tau c \beta}{128 \pi^2 \sigma^2 R^3} \csc\psi \exp\left(-\frac{a^2}{4\sigma^2} \tan^2\psi\right), \qquad (5.6.14)$$

and cross-section per unit area is

$$\sigma_o = K \frac{a^2}{\sigma^2} \exp\left(-\frac{a^2}{4\sigma^2} \tan^2\psi\right). \qquad (5.6.15)$$

For $a/\sigma = 10$, this calculation fits observed data between depression angles of 60° and 90°, but not at low depression angles.

6.0 CONCLUSION.

The existing theories can be divided into two general categories. The theories of the first group postulate a relatively simple mathematical model to describe the reflecting surface, and proceed with a more or less rigorous solution of the reflection and scattering from the surface. The theories of the second group describe the surface in terms of measurable quantities, and proceed to solve the problem of reflection and scattering from that surface. In general, the theories of the first group provide good solutions of the electromagnetic problem of scattering and reflection from the hypothesized surface, but the particular surface models often bear little resemblance to the actual surface of the earth. On the other hand, the theories of the second group encounter difficult problems when they attempt to find rigorous solutions from the electromagnetic field, but they have the advantage that, since they are formulated in terms of measurable surface quantities, their results can be more easily related to experimental data.

An evaluation or comparison of the existing theories is hampered by the fact that there is an insufficient quantity of experimental data with which to compare the theories to check their validity. For sea clutter, the facet

theory appears to be a more satisfactory explanation of radar back-scattering than either the corrugated surface or drop theories. The facet theory explains the frequency variation better than the drop theory, it provides a polarization dependence which the corrugated surface theory neglects, it accounts for the upwind-downwind ratio which the other two theories do not explain, and it gives quantitative results on the variation with wind which the other theories do not provide. The facet theory has not been extended to include the variation of radar area with time due to the fluctuations of the facet slopes.

For ground clutter, no theories have been devised which include an appreciable proportion of the existing types of earth surface. The two theories which seem to be most successful in their particular applications are the slightly rough surface theory applied to very smooth surfaces such as concrete or asphalt roads, and the lossy cylinder theory which can be applied to fields of tall grass. At the present time a general theory does not exist which can adequately describe the radar cross section of a general ground area in terms of the measurable physical properties of the area.

7.0 REFERENCES.

1. H. Goldstein, "A Primer of Sea Echo", U.S. Navy Electronics Laboratory Report 157, August 7, 1950, 30 pages.

2. E. W. Cowan, "X-Band Sea Return Measurements", Radiation Laboratory Report No. 870, Jan. 10, 1946, 20 pages.

3. H. Goldstein, "Frequency Dependence of the Properties of Sea Echo", Physical Review, Vol. 70, Nos. 11 and 12 (Dec. 1 & 15, 1946) pp. 938-946.

4. D. E. Kerr, "Propagation of Short Radio Waves", MIT Radiation Laboratory Series, Vol. 13, McGraw Hill Company, 1951, Chapter 6.

5. D. D. Crombie, "Doppler Spectrum of Sea Echo at 13.56 Mc/s", Nature, Vol. 175, No. 4459 (April 16, 1955), pp. 681-682.

6. F. C. Macdonald, "Characteristics of Radar Sea Clutter, Part I. Persistent Target-Like Echoes in Sea Clutter", Naval Research Laboratory Report No. 4902, March 19, 1957, 9 pages.

7. F. C. Macdonald, "The Correlation of Radar Sea Clutter on Vertical and Horizontal Polarization with Wave Height and Slope", IRE Convention Record, Vol. 4 Part I (1956) pp. 29-32.

8. F. C. Macdonald, "Recent Sea Clutter Measurements by NRL"; private communication.

9. W. S. Ament, J. A. Burkett, F. C. Macdonald, and D. L. Ringwalt, "Characteristics of Radar Sea Clutter: Observations at 220 megacycles", NRL Report 5218, November 19, 1958, 15 pages.

10. J. C. Wiltse, S. P. Schlesinger, C. M. Johnson, "Back Scattering Characteristics of the Sea in the Region from 10 to 50 kmc";

Proceedings of the IRE, Vol. 45 No. 2, (Feb. 1957) pp. 220-228.

11. R. P. Ingalls, "Measurements of Clutter Doppler Spectrum at Plum Island", MIT Lincoln Laboratory Memo, June 26, 1956, 7 pages.

12. C. A. Stutt, S. J. Fricker, R. P. Ingalls, M. L. Stone, "Preliminary Report on Ground-Wave Radar Sea Clutter", MIT Lincoln Laboratory Technical Report No. 134, Sept. 21, 1956, 27 pages.

13. C. R. Grant and B. S. Yaplee, "Back Scattering from Water and Land at Centimeter and Millimeter Wave Lengths", Proceedings of the IRE, Vol. 45 No. 7 (July 1957) pp. 976-982.

14. J. C. Boring, E. R. Flynt, M. S. Long, E. R. Widerquist, "Sea Return Study", Georgia Institute of Technology Engineering Experiment Station, Aug. 1, 1957, 108 pages.

15. B. L. Hicks, N. Knable, J. J. Kovaly, G. S. Newell, J. P. Ruina, "Sea Clutter Spectrum Studies Using Airborne Coherent Radar III", University of Illinois Control Systems Laboratory, Report R-105, May 1958, 31 pages.

16. R. C. Taylor, "Terrain Return Measurements at X, Ku and Ka bands", IRE National Convention Record, Part I, March 1959, pp. 19-26.

17. D. R. Bianse and C. S. Morris, "Radar Terrain Cross-Section at Microwave Frequencies", Paper delivered at Joint URSI-IRE meeting, Pennsylvania State University, October 21, 1958.

18. J. P. Campbell, "Back-Scattering Characteristics of Land and Sea at X-Band", General Precision Laboratory, Doppler Air Navigation Technical Series Report, Vol. 6, p. 10.

19. M. Katzin, "On the Mechanism of Radar Sea Clutter", Proceedings of the IRE, Vol. 45, No. 1, Jan. 1957, pp. 44-54.

20. M. Katzin "Sea Clutter At Large Depression Angles", Final Report, Contract No. Nonr-2138(00), 20 pages.

21. W. H. Peake, "Theory of Radar Return from Terrain", IRE National Convention Record, March 1959, Part I, pp. 28-32.

22. S. O. Rice, "Reflection of Electromagnetic Waves by Slightly Rough Surfaces", The Theory of Electromagnetic Waves(Symposium), Interscience Publishing Company, New York, 1951, pp. 351-378.

23. R. E. Clapp, "A Theoretical and Experimental Study of Radar Ground Return", MIT Radiation Laboratory Report No. 1024, 10 April 1946, pp. 20-22.

24. L. M. Spetner and I. Kata, "Radar Reflection From Land and Water Surfaces", Radar Return Symposium, U. of New Mexico, May 11, 1959.

25. C. Cox and W. Munk, "Statistics of the Sea Surface Derived From Sun Glitter", Journal of Marine Research, Vol. 13, No. 2, (Nov. 1, 1954), pp. 198-227.

26. H. Davies, "The Reflection Of Electromagnetic Waves From A Rough Surface", Proceedings of the IEE, Part IV Vol. 101, pp. 209-214 (August, 1954). Also, Discussion In Proc. IEE, Part C, Vol. 102, p. 148 (March, 1955).

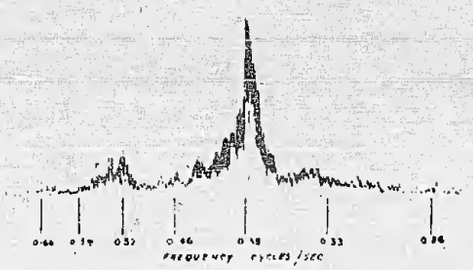

Fig. 1. Sea Clutter Spectrum

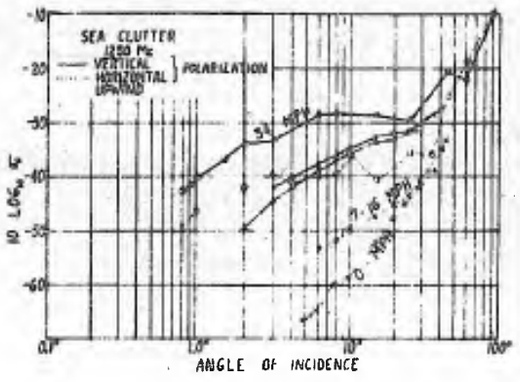

Fig. 2. Sea Clutter, L Band

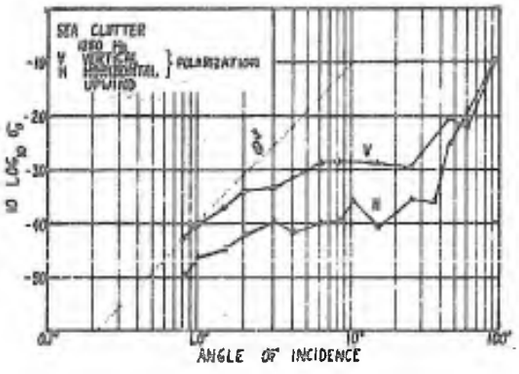

Fig. 3. Sea Clutter, L Band

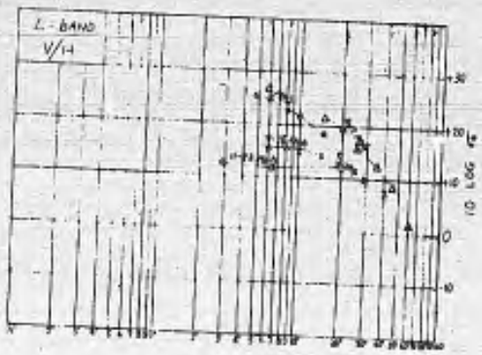

Fig. 4. Sea Clutter, V/H ratio, L Band

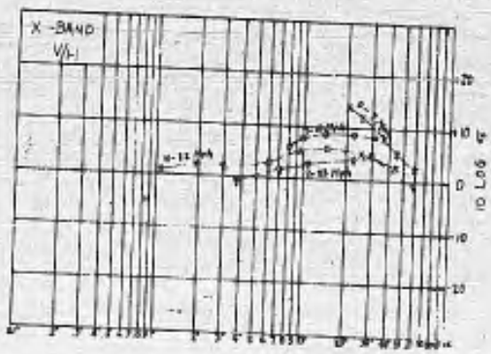

Fig. 5. Sea Clutter, V/H ratio, X Band

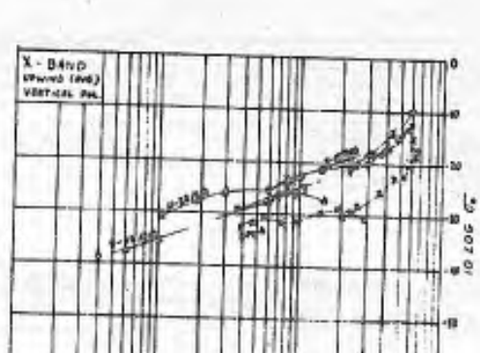

Fig. 6. Sea Clutter, X Band

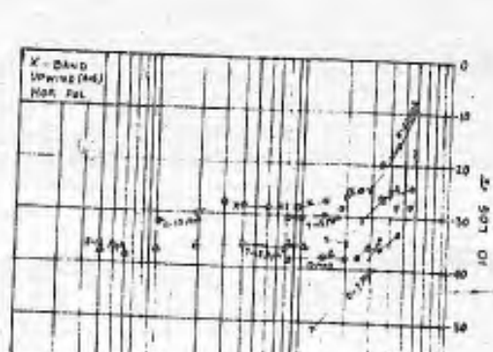

Fig. 7. Sea Clutter, X Band

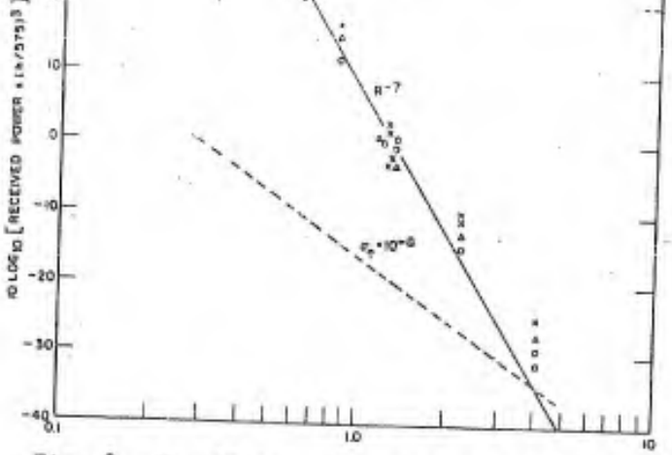

Fig. 8. Sea Clutter, Small depression angles

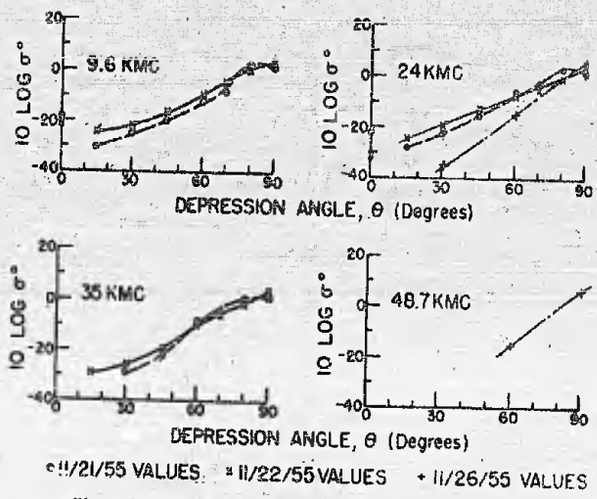

Plots of 10 log σ° vs depression angle for vertical polarization at four different microwave frequencies. The measurements for a particular day and depression angle were made simultaneously at all of the microwave frequencies indicated. (Sea moderate, wind speed 16 knots on November 21; sea moderately heavy, wind speed 26 knots on November 22; sea fairly calm, wind variable 4 to 10 knots on November 26.)

Fig. 9. Sea Clutter, 9.6 to 48.7 kmc.

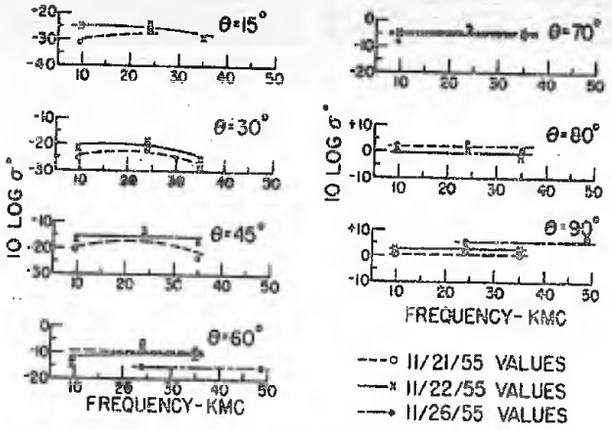

Variation of 10 log σ° with microwave frequency for different values of θ and for vertical polarization.

Fig. 10. Sea Clutter, frequency dependence.

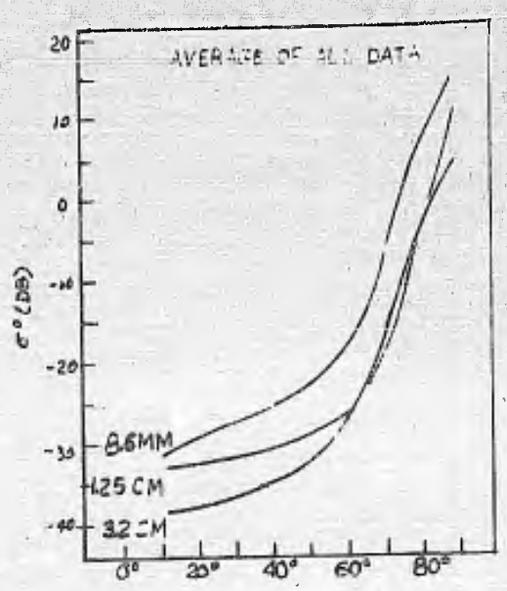

Fig. 11. Sea Clutter, 10 to 35 kmc.

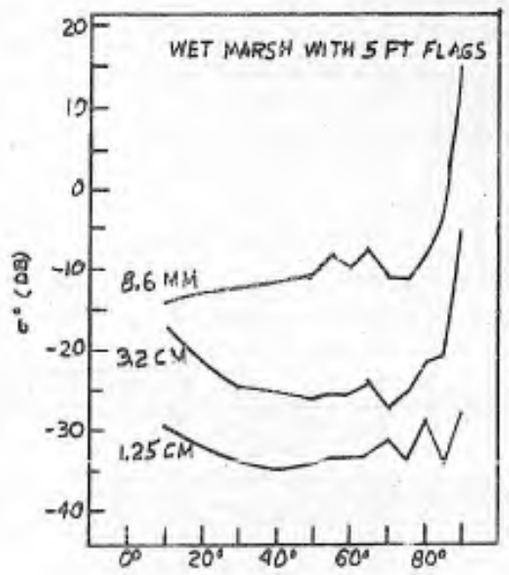

Fig. 12. Ground return, wet marsh land.

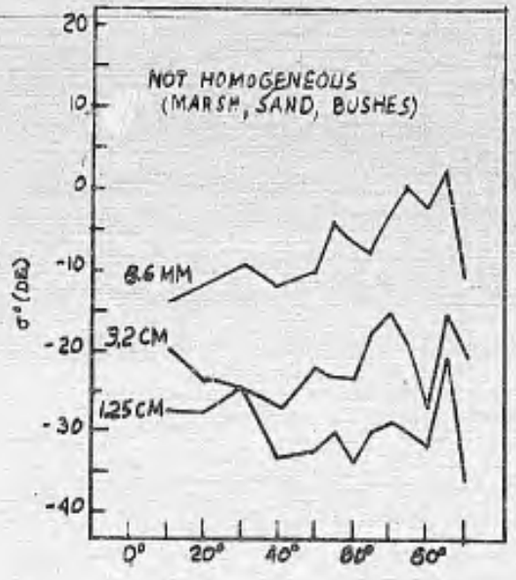

Fig. 13. Ground return; marsh, sand and bushes.

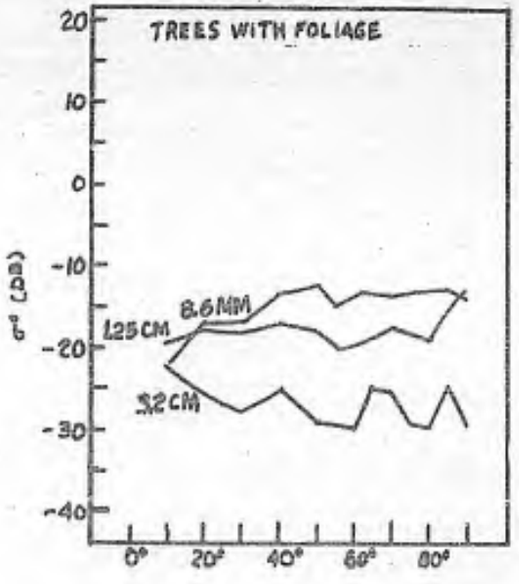

Fig. 14. Ground return, trees with foliage.

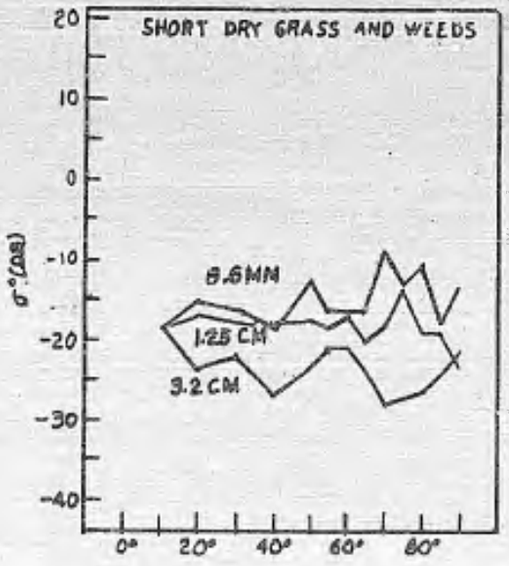

Fig. 15. Ground return, short dry grass and weeds.

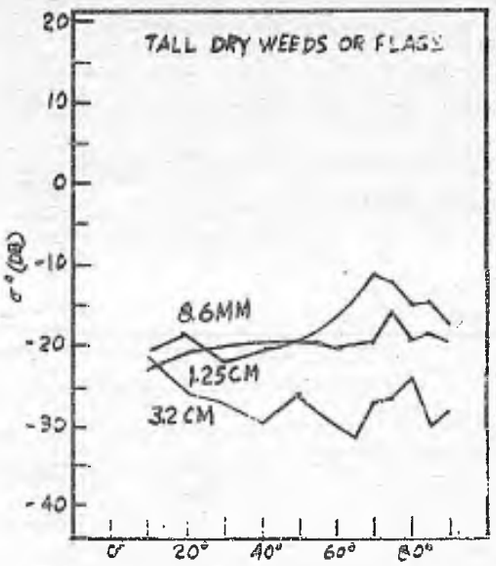

Fig. 16. Ground return, tall grass.

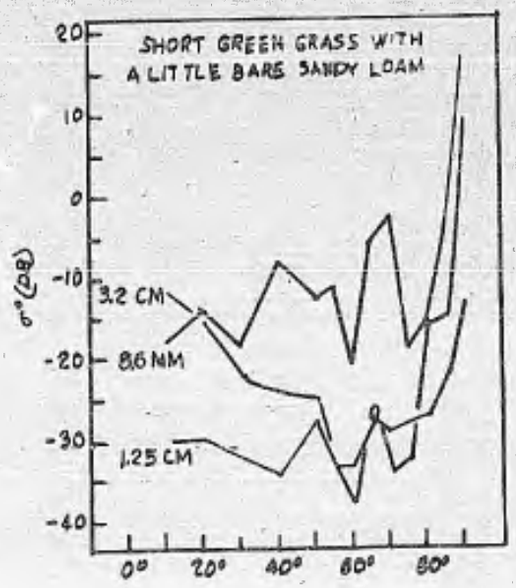

Fig. 17. Ground return, short green grass.

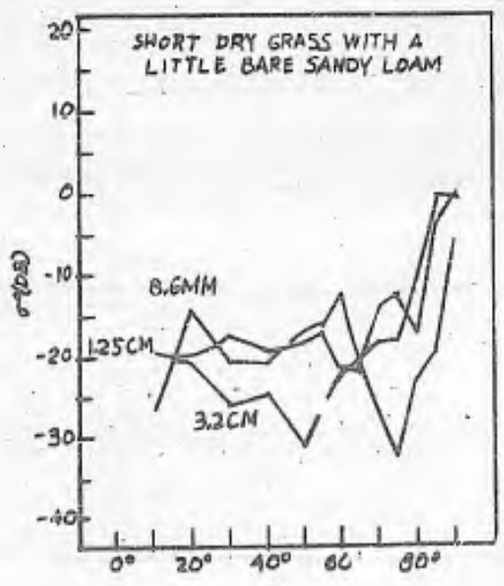

Fig. 18. Ground return, short dry grass.

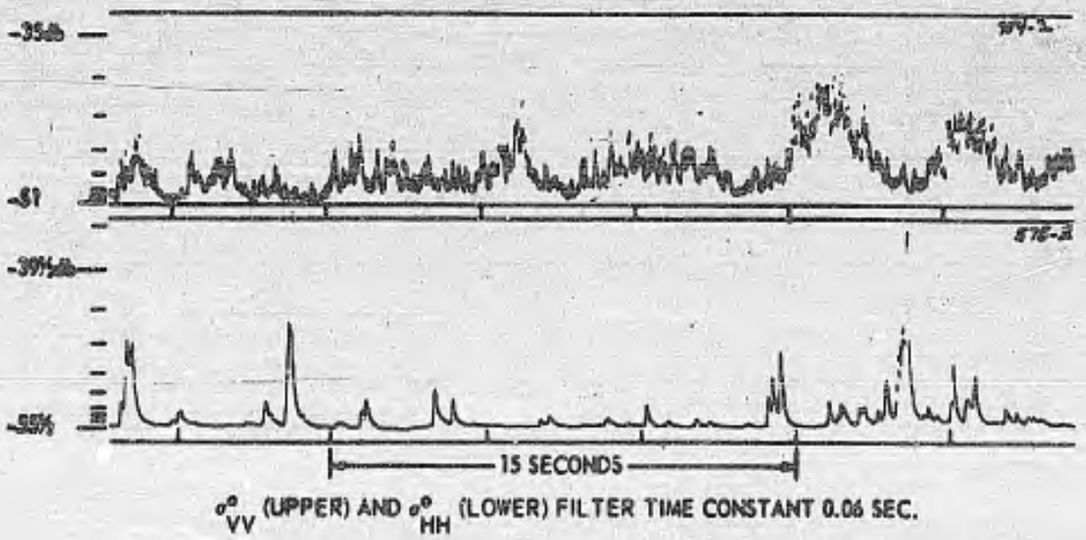

σ°_{VV} (UPPER) AND σ°_{HH} (LOWER) FILTER TIME CONSTANT 0.06 SEC.

Fig. 19. Sea Clutter fluctuations.

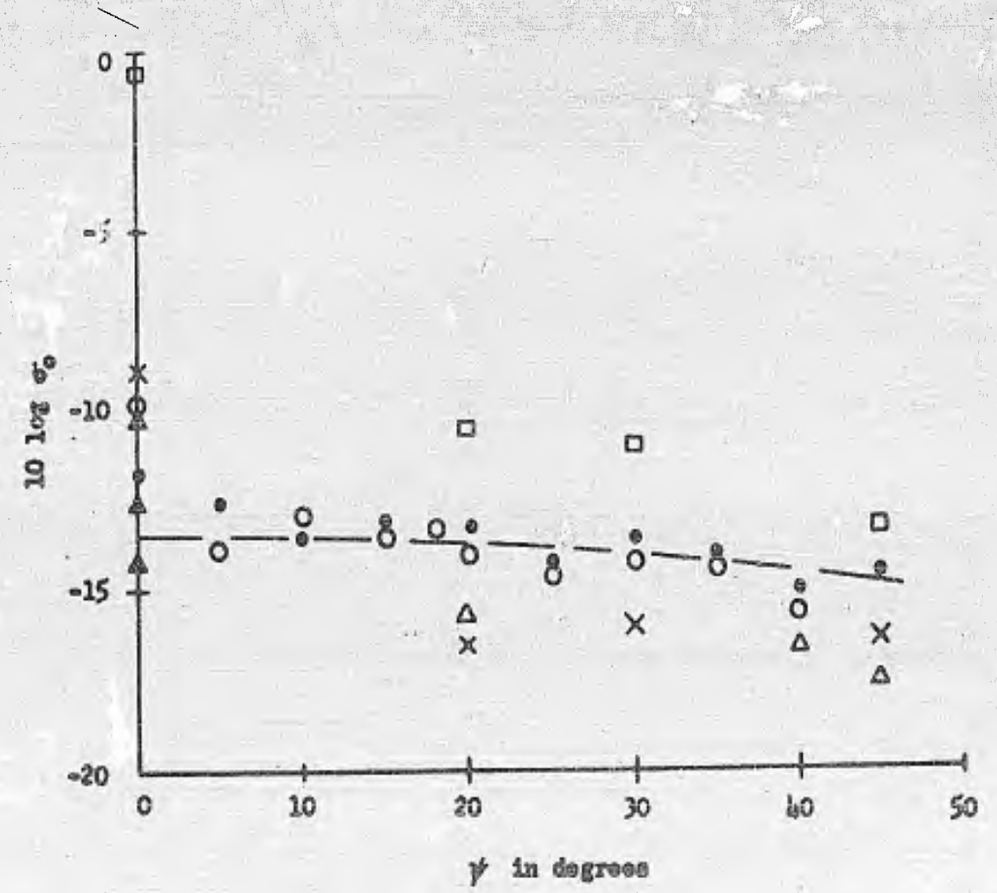

Scattering cross-section at X-band vs. incidence angle, for land (1953 experiments). Averages of measurements with horizontal and vertical polarization are given. The dashed curve represents "isotropic" terrain. Symbols: O Wooded land (New Jersey); ● wooded land(Connecticut); × cultivated land(Virginia); □ Long Island; △ Philco sites (see text).

Fig. 20. Ground return, woods and cultivated fields.

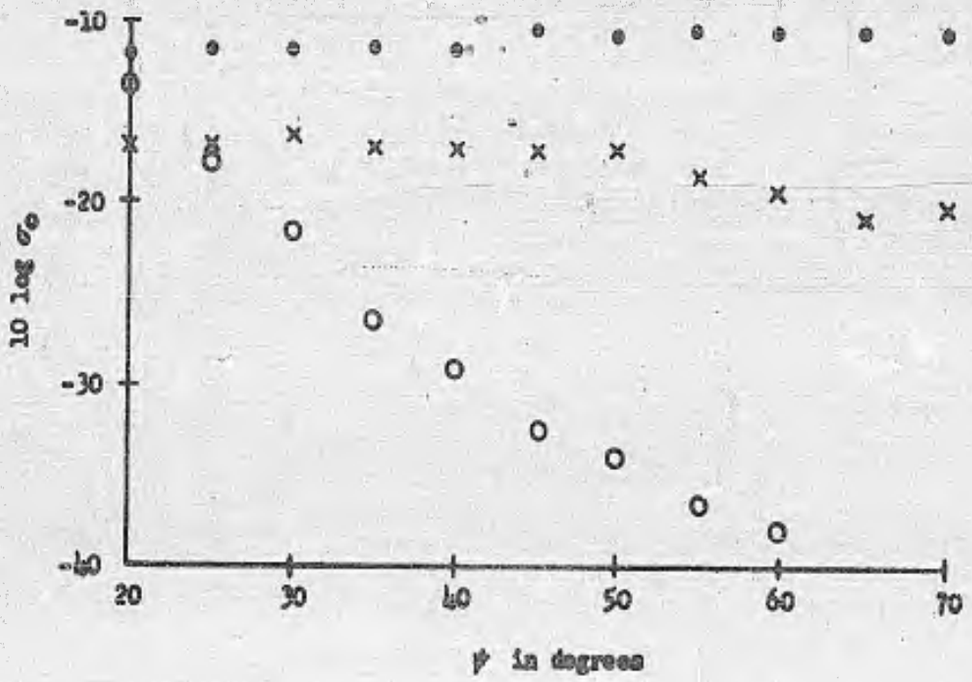

Scattering cross-section vs. incidence angle (1947-48 experiments). The measurements were made at X-band with horizontal polarization. Symbols: • wooded land (Connecticut); × cultivated land (Virginia); ○ Atlantic Ocean, Beaufort 2-3.

Fig. 21. Ground return, marsh and cultivated fields.

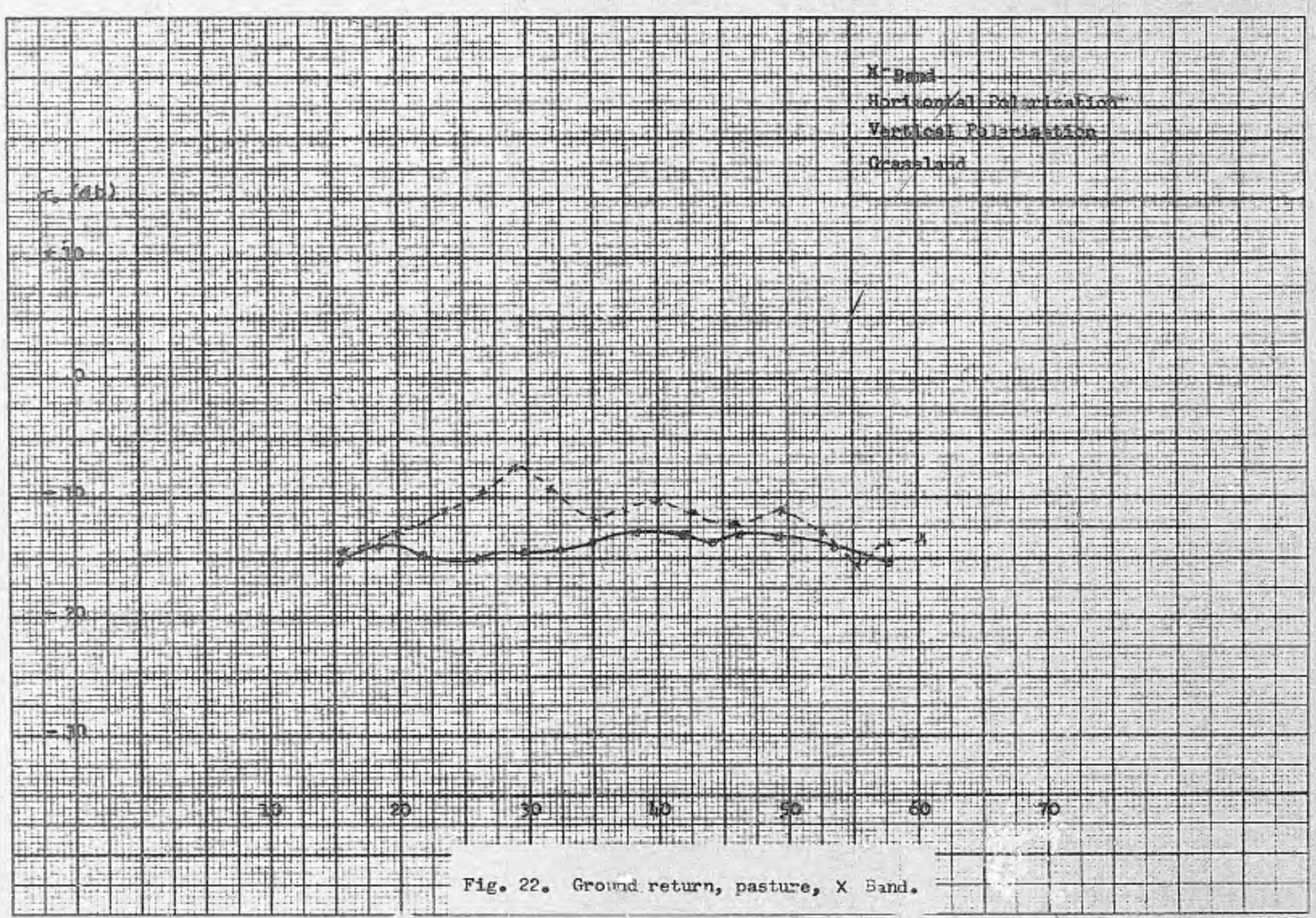

Fig. 22. Ground return, pasture, X Band.

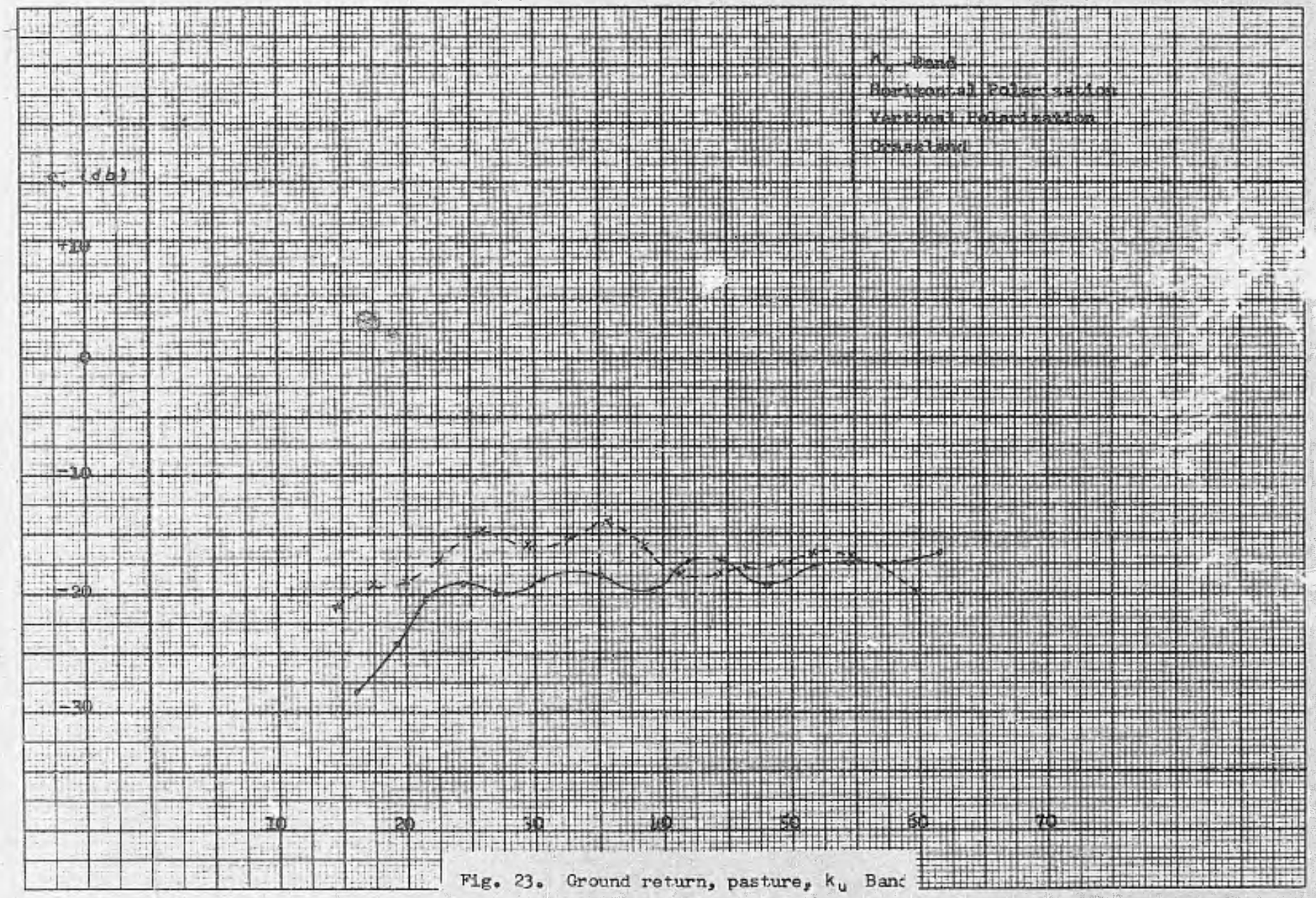

Fig. 23. Ground return, pasture, k_u Band

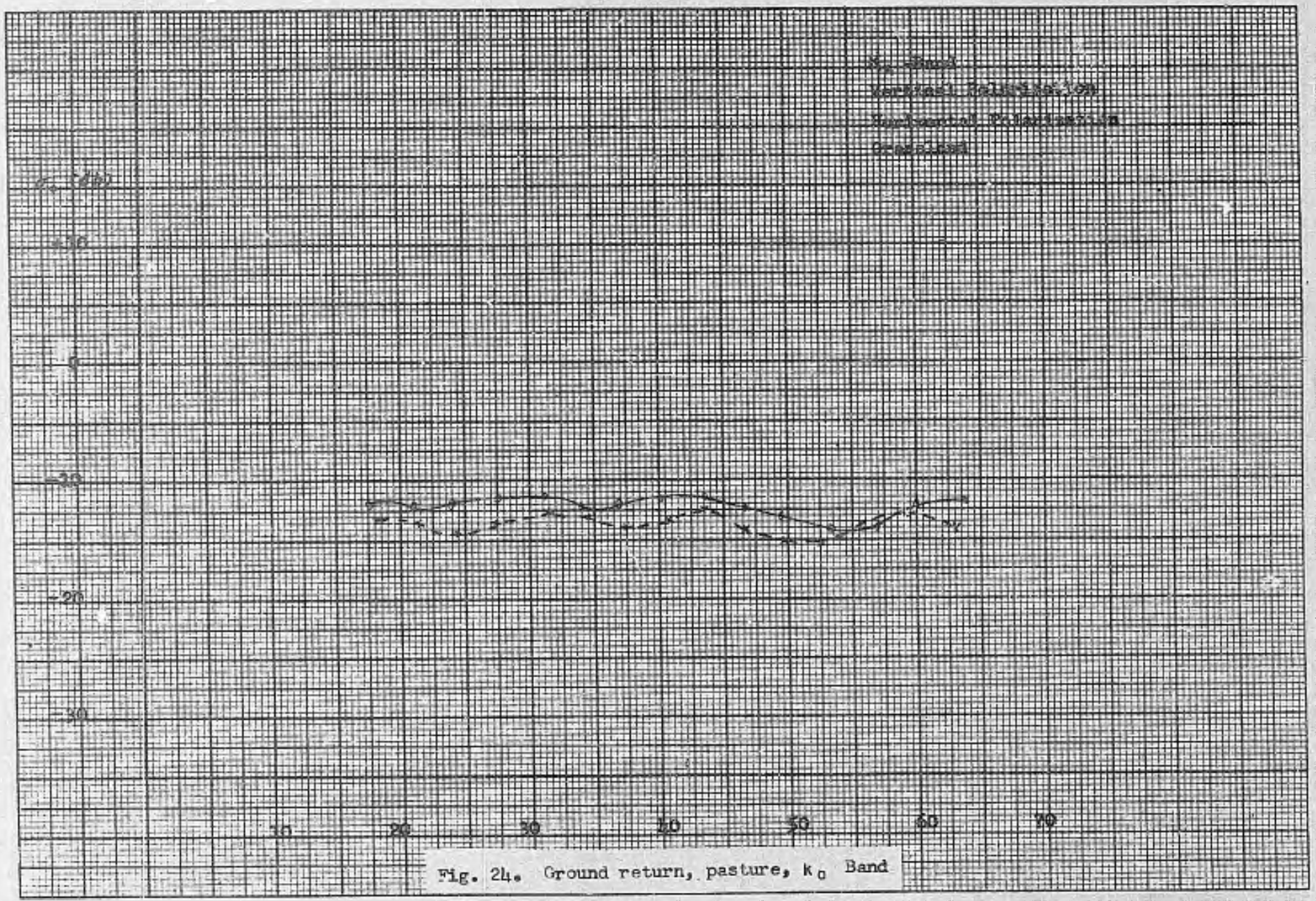

Fig. 24. Ground return, pasture, k_0 Band

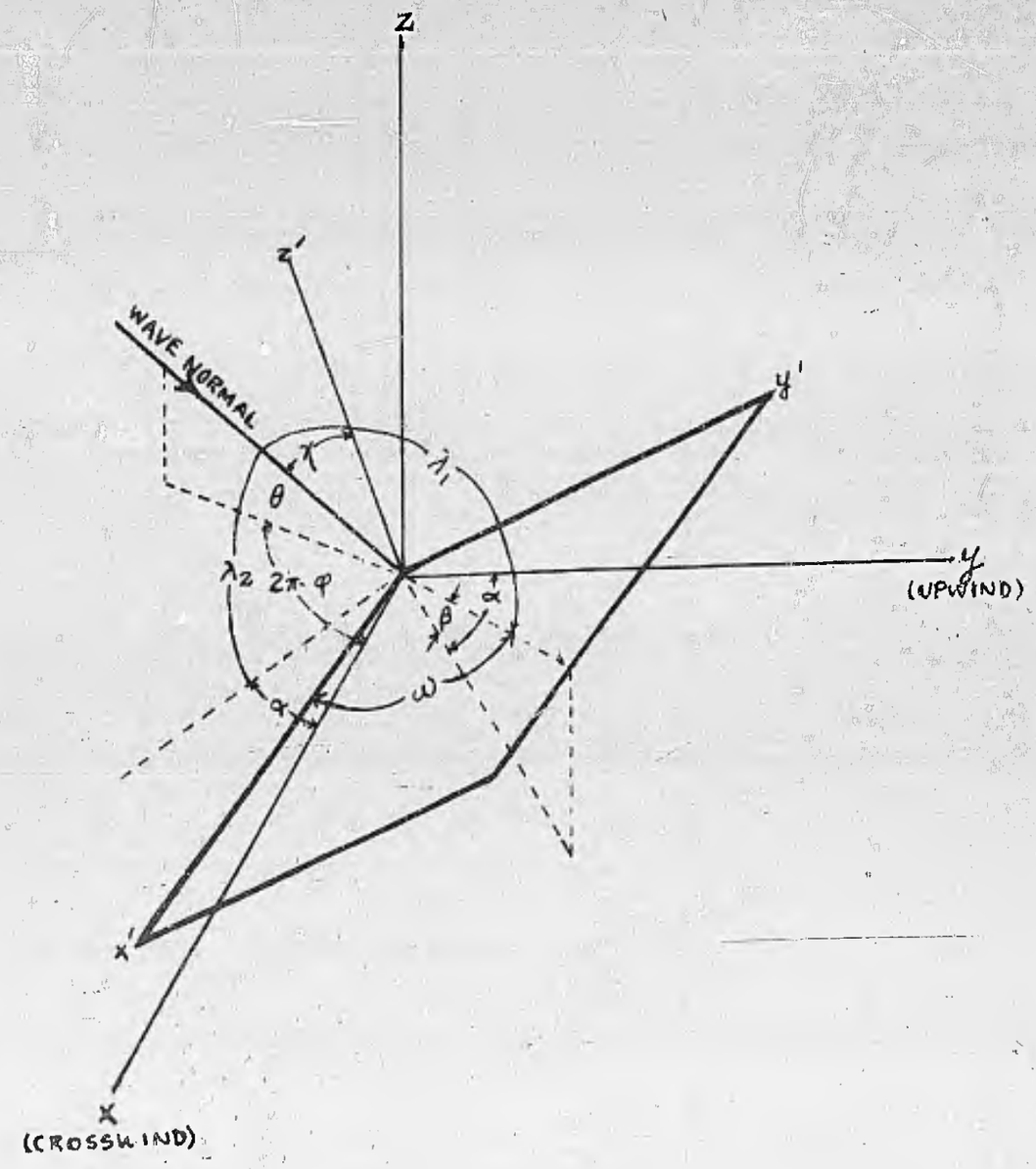

Fig. 25. Geometry for facets.

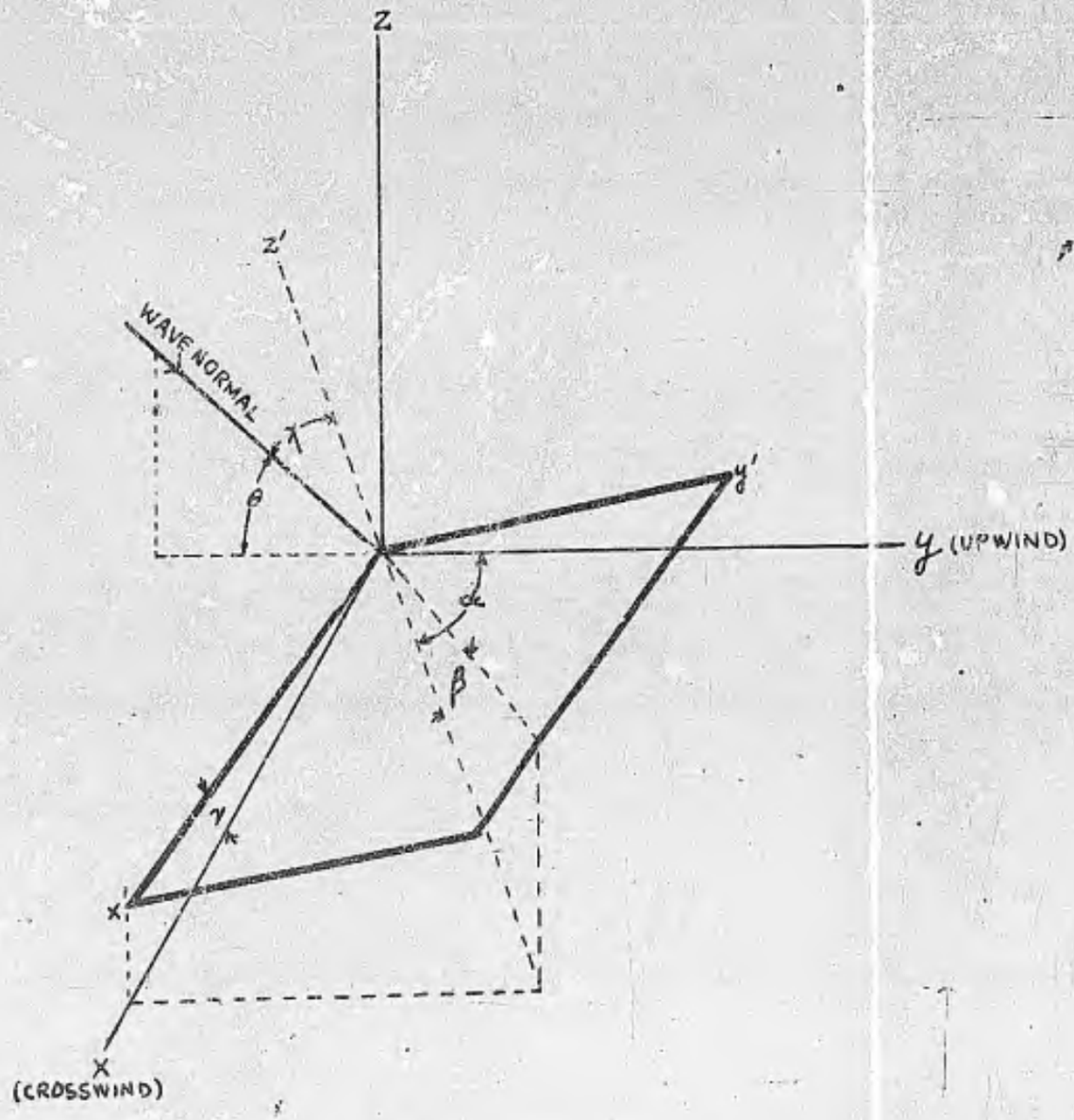

Fig. 26. Geometry for facets aligned with the wind.